AIMS Mathematics, 11(5): 12500–12533.
DOI: 10.3934/math.2026514
Received: 12 February 2026
Revised: 15 April 2026
Accepted: 24 April 2026
Published: 06 May 2026

https://www.aimspress.com/journal/Math

Research article

Three-dimensional adaptive guidance law for a missile delivering a deployable sonar device under impact velocity and angle constraints

Jian Huang, Zhanpeng Gao, Jun Liu and Wenjun Yi*

National Key Lab of Transient Physics, Nanjing University of Science and Technology, Nanjing 210094, China

* **Correspondence:** Email: wenjunyi@njust.edu.cn.

Abstract: Sonar detection is a cornerstone capability in anti-submarine warfare, where the remote and accurate deployment of sensing devices must be completed within the shortest possible time. To this end, this paper proposes a missile-based concept for delivering a deployable sonar device and develops a three-dimensional adaptive guidance law with fixed-time convergence. To reduce the impact kinetic energy at water entry and to deploy the deployable sonar device with a prescribed attitude, constraints on the impact velocity and impact angle are explicitly imposed. To avoid the range unreachability induced by deceleration-based guidance laws and to prevent excessive flight time, a two-phase guidance strategy with smooth switching is devised along the line-of-sight direction. To further enhance the stability of the guidance process, an adaptive term is incorporated into the double-power reaching law to alleviate the acceleration saturation that may occur during the initial guidance stage. Simulation results demonstrate that, under the proposed guidance law, the missile can accurately reach the target with the desired impact velocity and impact angle, while alleviating early-stage acceleration saturation and effectively reducing the load on the onboard actuators. Consequently, this study provides a feasible solution for delivering the deployable sonar device with favorable maneuverability and flexible deployment capability, and it shows certain potential in adapting to different meteorological conditions, reducing reliance on real-time human intervention, and improving missions execution efficiency.

Keywords: missile delivering a deployable sonar device; adaptive term; two-phase guidance strategy; impact velocity constraint; impact angle constraint; guidance law; sliding mode control
Mathematics Subject Classification: 93D05, 93D40

1. Introduction

In modern navies, with the growing development and expansion of underwater military forces such as submarines, anti-submarine warfare has become increasingly important [1]. Owing to the limited detection range of shipborne sonar and the progressive degradation of detection accuracy with increasing distance, shipborne sonar alone can hardly satisfy the mission requirements for long-range detection of underwater targets. Current research efforts have focused on deploying sonar detection devices into the target sea area using anti-submarine helicopters or unmanned aerial vehicles, so as to localize and track potential military objects [2–5]. However, anti-submarine helicopters and unmanned aerial vehicles are vulnerable to threats from surface-to-air missiles during mission execution and are also susceptible to meteorological constraints. In addition, the relatively long preparation time required for anti-submarine helicopters and unmanned aerial vehicles makes it difficult to respond to time-critical anti-submarine warfare missions. Therefore, this paper proposes a missile-based concept for delivering a deployable sonar device. Compared with conventional anti-submarine helicopter and unmanned aerial vehicle platforms, this approach offers higher maneuverability and a faster response, and it exhibits potential mission adaptability under different meteorological conditions. In addition, it is expected to reduce reliance on real-time human involvement during mission execution, thereby mitigating efficiency loss due to manual operation.

Several key issues must be addressed when designing a guidance law for the considered missile delivering a deployable sonar device. First, the deployable sonar device should be arranged in an appropriate array configuration to enable accurate localization of underwater targets [6, 7]. Therefore, the missile must reach the prescribed deployment point with high precision. Second, the high acceleration loads encountered during flight may impose substantial stress on the onboard actuators. To mitigate this issue, the guidance law should avoid possible acceleration saturation throughout the flight. Moreover, excessive impact loads at water entry may damage the deployable sonar device. Numerous studies have shown that the impact angle and impact velocity at water entry significantly affect the impact load experienced by the body. Specifically, a smaller entry angle relative to the water surface and a lower velocity result in a reduced impact load during impact [8–11]. Accordingly, the proposed guidance law must explicitly enforce both the impact angle constraint and the impact velocity constraint.

Recent studies on intermittent control and event-triggered control for complex dynamical systems have enriched the theoretical background of constrained control design [12,13]. Meanwhile, constraint-aware sliding-mode-based schemes have also been actively developed to address input magnitude and rate saturations as well as compound uncertainties in practical systems [14, 15]. In addition, recent studies on data-driven sliding mode control have further demonstrated the strong disturbance-rejection capability of sliding-mode-based designs for uncertain nonlinear systems, thereby broadening the theoretical background of robust constrained control [16, 17]. Robustness-oriented guidance research has also explored joint guidance-and-control design under model uncertainty and real-time fault-tolerant guidance under degraded conditions, which provides useful background for robustness enhancement, although its problem setting differs from the terminal velocity/impact-angle constrained delivery scenario considered here [18, 19]. Against this broader background, sliding mode control has been extensively used in the design of guidance laws with terminal angle constraints due to its strong robustness [20–22]. Wang et al. [23] developed a time-varying sliding surface that effectively

reduced the impact angle error and miss distance without violating the field-of-view constraint. Gao et al. [24] combined proportional–integral–derivative control with sliding mode control and performed parameter tuning using intelligent optimization algorithms, thereby improving the accuracy and disturbance rejection capability of the guidance and control system. Zheng et al. [25] proposed a periodic time-delay sliding surface to guarantee the prescribed-time convergence of both the LOS tracking error and the LOS angular rate. Wang et al. [26] presented a sliding mode guidance law achieving finite-time convergence, where terminal angle constraints, second-order autopilot dynamics, and input saturation constraints were explicitly incorporated. Although these studies are limited to two-dimensional planar engagements, they provide important insights for the design of three-dimensional guidance laws with terminal angle constraints. Dong et al. [27] considered the impact angle constraint, derived the relationship between the impact angles and the terminal LOS angles in three-dimensional space, and proposed a nonsingular terminal sliding mode cooperative guidance law under impact angle constraints. Hu et al. [28] integrated reinforcement learning with nonsingular terminal sliding mode theory to further reduce the miss distance and impact angle error. In addition, some studies have designed guidance laws by combining terminal angle constraints with various operational requirements. Yang et al. [29] proposed a nonsingular three-dimensional impact angle guidance strategy under physical constraints based on nonlinear coupled engagement kinematics. This method does not require decoupling the system into two subsystems, while simultaneously satisfying the impact angle constraints and the field-of-view limit. Hou et al. [30] developed a nonlinear three-dimensional all-aspect guidance law, which can still enable the missile to intercept the target with the desired impact angles even in the presence of large initial pointing errors. Gao et al. [31] designed a novel nonlinear proportional–integral–derivative sliding surface, based on which the resulting guidance law can engage maneuvering targets with the prescribed attack time and attack angles. In existing studies on guidance law design, most efforts focus on angle constraints and remaining flight-time constraints [32–34], whereas relatively few works explicitly address guidance laws with impact velocity constraints.

In practical operations, imposing an impact velocity constraint can enable a missile to fulfill its tactical requirements more effectively, and related studies have given this increasing attention in recent years. Li et al. [35] proposed a three-dimensional cooperative guidance algorithm with fixed-time convergence, which regulates the impact velocity of multiple missiles while ensuring that they attack the target with the desired angles, and exhibits strong disturbance rejection capability. The three-dimensional fault-tolerant cooperative guidance law proposed by Gao et al. [36] also imposes constraints on both the impact velocity and impact angles, thereby further enhancing the strike capability and stability of missile swarms. In addition, several studies, although not explicitly aimed at impact velocity constraint enforcement, incorporate acceleration regulation along the LOS direction [37–40]. Among the existing studies involving impact velocity constraints, most are intended to increase the terminal impact velocity to enhance lethality, and few have addressed guidance law design for reducing the missile–target relative velocity. More importantly, when simultaneously enforcing impact velocity and impact angle constraints, these methods may lead to acceleration saturation, which does not meet the design requirements of the guidance law for a missile delivering a deployable sonar device.

Therefore, this paper proposes a three-dimensional adaptive guidance law subject to both impact velocity and impact angle constraints for a missile delivering a deployable sonar device. In designing

the sliding mode guidance law, the sliding surface adopted in [41–43] is utilized, and an adaptive gain is further introduced into the double-power reaching law [27] to enhance the stability of the guidance process. For the guidance law along the LOS direction, a two-phase control framework is adopted: The first phase avoids deceleration, whereas the second phase enforces the constraint on the missile–target relative velocity. During phase switching, the smoothly varying function designed in this paper is introduced to achieve a bumpless transfer, thereby avoiding abrupt changes in the guidance command. The resulting guidance law enables the missile to rapidly and accurately reach the target with the desired impact velocity and impact angle in a stable manner, while reducing the burden on the onboard actuators.

The main contributions of this paper are summarized as follows.

1. This paper, for the first time, proposes a missile-based concept for delivering a deployable sonar device, which demonstrates certain advantages in maneuverability and flexible deployment and has potential application value in adapting to different meteorological conditions, reducing reliance on real-time human intervention, and improving mission responsiveness.
2. A two-phase guidance strategy is developed for the guidance law along the LOS direction. This strategy avoids any range unreachability caused by deceleration-based guidance laws and significantly shortens the missile flight time, thereby ensuring mission efficiency for sonar detection. Meanwhile, a smoothly varying function is designed to achieve a bumpless transfer when switching the LOS guidance law, thus avoiding abrupt jumps in the acceleration command.
3. An adaptive term is incorporated into the double-power reaching law to regulate the control demand in the initial phase with large errors. The novelty lies not merely in using a double-power reaching law itself, but in constructing a smooth adaptive gain related to time, error magnitude, and relative distance, to alleviate the early-stage control peak under the considered mission requirements.
4. The proposed guidance law achieves fixed-time convergence, i.e., the settling time is determined solely by the system's parameters and is independent of the initial conditions. This property ensures that the guidance system can converge stably and rapidly under complex and time-varying battlefield environments. Verification results show that the proposed guidance law enables the missile to rapidly and accurately reach the target with the desired impact velocity and impact angle in a stable manner, while reducing the burden on the onboard actuators.

The remainder of this paper is organized as follows. Section 2 formulates the problem and presents the engagement kinematics and guidance law model. Section 3 details the proposed guidance law design. Section 4 provides four groups of simulation results. Section 5 concludes the paper and outlines future research directions.

2. Problem formulation, engagement kinematics, and guidance law model

2.1. Problem formulation

Anti-submarine warfare may involve various time-critical contingencies, and the missile delivering a deployable sonar device is required to accomplish accurate deployment within the shortest possible time to enable the localization and tracking of underwater targets. In addition, large acceleration loads may arise throughout the flight, imposing considerable stress on the onboard actuators. To address

this issue, acceleration saturation in the guidance subsystems should be avoided. Meanwhile, the impact velocity and impact angle at water entry must be constrained to reduce the impact load, thereby alleviating the burden on the onboard actuators.

Accordingly, the guidance law developed in this paper is required to enable the missile to rapidly and accurately reach the target with the desired impact velocity and impact angle in a stable manner, while avoiding possible acceleration saturation during the flight.

2.2. Relevant lemmas

Lemma 1. [44,45] *Consider the following nonlinear system:*

$$\dot{x} = f(x,t), \quad f(0,t) = 0 \tag{2.1}$$

where $f : D \to R^n$ is a locally Lipschitz mapping, and suppose that $V(x)$ is a smooth positive-definite function on $U \subset R^n$. If $\forall \beta_1 > 0$, $\beta_2 \in (0,1)$ satisfy

$$\dot{V}(x) + \beta_1 V^{\beta_2}(x) \leq 0, \tag{2.2}$$

then the settling time $T(x)$ satisfies

$$T(x) \leq \frac{V^{1-\beta_2}(x)}{\beta_1 (1-\beta_2)}. \tag{2.3}$$

2.3. Engagement kinematics

The geometric schematic of launching the missile delivering a deployable sonar device is shown in Figure 1. M denotes the centroid of the missile's body; T denotes the target point; $OX_LY_LZ_L$ denotes the LOS reference coordinate system; $OX_IY_IZ_I$ denotes the inertial reference frame; $OX_MY_MZ_M$ denotes the trajectory coordinate system of the missile delivering a deployable sonar device, r denotes the relative distance between the missile and the target, V_M denotes the missile velocity vector; θ_L, ϕ_L denote the LOS elevation angle and the LOS azimuth angle, respectively; and ϑ_M, ψ_M denote the missile pitch angle and yaw angle, respectively.

The kinematic equations of the missile delivering a deployable sonar device are given in Eq (2.4)

$$\begin{cases} \dot{X}_M = V_M \cos\vartheta_M \cos\psi_M \\ \dot{Y}_M = V_M \sin\vartheta_M \\ \dot{Z}_M = -V_M \cos\vartheta_M \sin\psi_M \\ \dot{\vartheta}_M = \dfrac{a_{My}}{V_M} \\ \dot{\psi}_M = -\dfrac{a_{Mz}}{V_M \cos\vartheta_M} \\ \dot{V}_M = a_{Mx} \end{cases}. \tag{2.4}$$

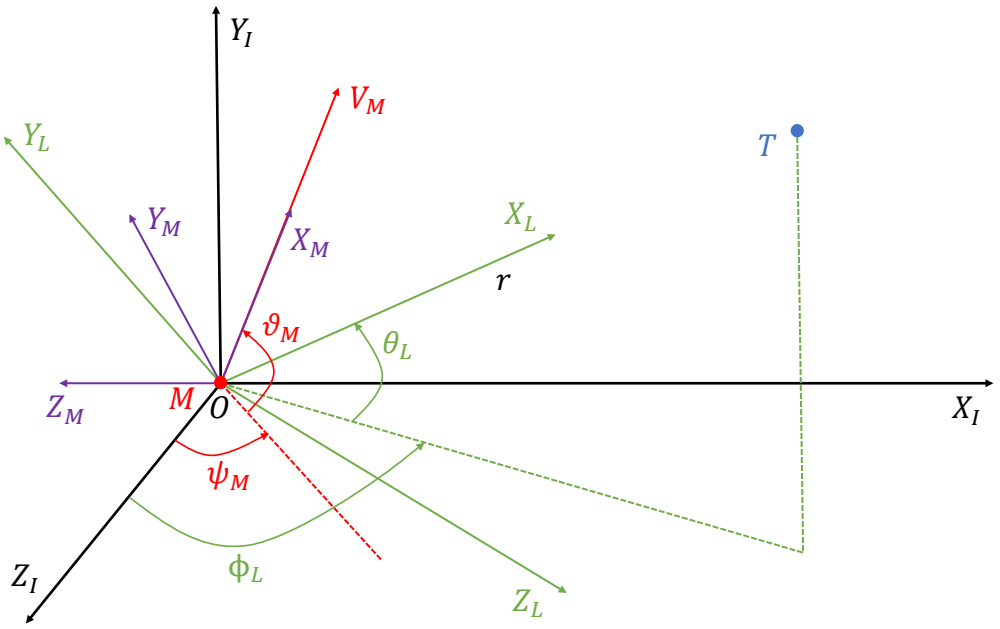

Figure 1. Relative motion geometry between the missile delivering a deployable sonar device and the target.

In Eq (2.4), (X_M, YM, Z_M) denotes the missile's position in the LOS inertial reference frame; a_{Mx}, a_{My}, a_{Mz} denote the missile's accelerations in the mutually orthogonal planes, respectively. The corresponding relative kinematic equations in the LOS reference frame are given as follows:

$$\ddot{r} - r\dot{\theta}_L^2 - r\dot{\phi}_L^2 \cos^2\theta_L = -a_{Mr} \tag{2.5}$$

$$r\ddot{\theta}_L + 2\dot{r}\dot{\theta}_L + r\dot{\phi}_L^2 \sin\theta_L \cos\theta_L = -a_{M\theta} \tag{2.6}$$

$$-r\ddot{\phi}_L \cos\theta_L - 2\dot{r}\dot{\phi}_L \cos\theta_L + 2r\dot{\theta}_L\dot{\phi}_L \sin\theta_L = -a_{M\phi}. \tag{2.7}$$

In the equations above, $a_{Mr}, a_{M\theta}, a_{M\phi}$ denote the acceleration components of the missile in the LOS reference frame, respectively.

2.4. Guidance law model

To reduce the impact load experienced by the missile delivering a deployable sonar device at water entry and to prevent damage to the deployable sonar device, the water-entry velocity of the missile should be reduced. Meanwhile, to ensure that the deployable sonar device can be deployed successfully, the water-entry angle of the missile must be constrained. Therefore, the guidance law for the missile delivering a deployable sonar device is designed in three directions, i.e., the LOS direction, the LOS normal direction, and the LOS lateral direction. Define $x_1 = r, x_2 = \dot{r}, x_3 = \theta_L - \theta_{Ld}, x_4 =$

$\dot{\theta}_L, x_5 = \phi_L - \phi_{Ld}$, and $x_6 = \dot{\phi}_L$. Here, θ_{Ld}, ϕ_{Ld} denote the desired water-entry angles of the missile. Combining Eqs (2.5)–(2.7), the state-space representation of the system is given by

$$\begin{cases} \dot{x}_1 = x_2, \\ \dot{x}_2 = x_1 x_4^2 + x_1 x_6^2 \cos^2\theta_L - a_{Mr}, \\ \dot{x}_3 = x_4, \\ \dot{x}_4 = -\dfrac{2x_2 x_4}{x_1} - x_6^2 \sin\theta_L \cos\theta_L - \dfrac{a_{M\theta}}{x_1}, \\ \dot{x}_5 = x_6, \\ \dot{x}_6 = -\dfrac{2x_2 x_6}{x_1} + 2x_4 x_6 \tan\theta_L + \dfrac{a_{M\phi}}{x_1 \cos\theta_L}. \end{cases} \tag{2.8}$$

In accordance with the design requirements of the missile delivering a deployable sonar device, x_1, x_3, x_4, x_5, x_6 are required to converge to 0, while x_2 is required to converge to the desired terminal velocity, so that the missile can reach the target with the prescribed impact velocity and impact angles. The specific control objective is given in Eq (2.9)

$$\begin{cases} \lim\limits_{t\to T_f} x_1 = 0, \quad \lim\limits_{t\to T_f} x_2 = V_d, \\ \lim\limits_{t\to T_f} x_3 = 0, \quad \lim\limits_{t\to T_f} x_4 = 0, \\ \lim\limits_{t\to T_f} x_5 = 0, \quad \lim\limits_{t\to T_f} x_6 = 0, \end{cases} \tag{2.9}$$

where V_d denotes the desired water-entry velocity of the missile, and T_f denotes the actual flight time of the missile.

3. Sliding mode guidance law design for the missile delivering a deployable sonar device

This chapter designs the guidance law for the missile delivering a deployable sonar device in two parts. A deceleration guidance law is developed along the LOS direction, while impact angle constrained guidance laws are designed in the LOS normal and LOS lateral directions.

3.1. Design of the LOS direction deceleration sliding mode guidance law

To achieve deceleration guidance of the missile along the LOS direction, the sliding surface is designed as follows:

$$s_1 = x_2 - V_d. \tag{3.1}$$

Taking the time derivative of both sides of Eq (3.1) yields

$$\dot{s}_1 = \ddot{r}. \tag{3.2}$$

In this paper, the double-power reaching law [27] is adopted as the baseline, as given in Eq (3.3)

$$\dot{s} = -l_1 |s|^{p_1} \operatorname{sgn}(s) - l_2 |s|^{p_2} \operatorname{sgn}(s). \tag{3.3}$$

In Eq (3.3), l_1, l_2, p_1, p_2 are all positive parameters. At the initial stage of guidance, the large initial error leads to a large magnitude of the sliding variable s_1 in Eq (3.1). Consequently, the term $-l_1|s|^{p_1}\,\mathrm{sgn}(s)$ in the reaching law also increases, thereby enabling rapid error reduction and convergence to the sliding surface. As a result, a large acceleration command may be generated in the early guidance stage, which can cause acceleration saturation and abrupt jumps in the acceleration command. To further reduce the load on the onboard actuators and enhance the stability of the guidance process, an adaptive term is introduced into the double-power reaching law. This adaptive term alleviates any early-stage acceleration saturation induced by large initial errors, reduces the load on the onboard actuators, and improves the stability of the guidance process.

To construct the adaptive term, $\bar{s}_k$ and $\bar{r}_k$ are first introduced as the historical averages of the sliding variable and the missile–target relative distance, respectively

$$\bar{s}_k = \bar{s}_{k-1} + \alpha\left(|s_k| - \bar{s}_{k-1}\right) \tag{3.4}$$

$$\bar{r}_k = \bar{r}_{k-1} + \alpha\left(|r_k| - \bar{r}_{k-1}\right), \tag{3.5}$$

where k denotes the discrete time index and $\alpha = 0.05$. This formulation converts instantaneous quantities into variables with a relative-scale interpretation, thereby establishing an adaptive reference scale for the system operating condition.

To characterize the variation trend of the current state relative to the "normal operating level", d_s and d_r are introduced as the deviation measures of the sliding variable and the missile–target relative distance, respectively

$$d_s = \frac{|s_k| - \bar{s}_k}{\bar{s}_k + \varepsilon_s} \tag{3.6}$$

$$d_r = \frac{|r_k| - \bar{r}_k}{\bar{r}_k + \varepsilon_r}. \tag{3.7}$$

In the above equations, when $d_s > 0$, the error is amplified and the system may deviate from the sliding surface; when $d_s < 0$, the error decreases and the system tends to be stable. The same interpretation applies to d_r. This normalized form ensures consistent algorithmic behavior for systems with different physical dimensions and magnitudes, thereby improving generality and robustness.

To enable adaptive weight adjustment, w_s^{ad} and w_r^{ad} are introduced in Eqs (3.8) and (3.9), respectively. A *tanh* function is used to smoothly map the deviation measures so that the weights vary continuously with the deviation level, without abrupt changes. Specifically, the adjustment strength is automatically increased when the deviation is large, whereas the excitation level is automatically reduced when the system operates steadily, thereby avoiding excessive control

$$w_s^{ad} = w_s\left(1 + 0.5\,\tanh(d_s)\right) \tag{3.8}$$

$$w_r^{ad} = w_r\left(1 + 0.3\,\tanh(d_r)\right). \tag{3.9}$$

In the equations above, $w_s = 2$ and $w_r = 0.1$. This design avoids the chattering issue typically induced by conventional switching-type or piecewise adaptive laws, and renders the gain variation continuous and differentiable.

To prevent excessive acceleration spikes in the early guidance stage, three excitation terms, e_t, e_s, and e_r, are constructed for the adaptive gain based on time progression, sliding-mode driving, and distance suppression, respectively

$$e_t = w_t (t - t_{\text{ref}}) \tag{3.10}$$

where $w_t = 1$ and $t_{\text{ref}} = 10$. The time excitation term is introduced to provide a global convergence-driving effect. At the initial stage of control, the gain remains small to avoid excessive initial transients; as time evolves, the control effort is gradually strengthened. Therefore, this excitation term ensures that the gain can still increase progressively even when the error signal is small but convergence has not been achieved over an extended period.

$$e_s = w_s^{ad} \frac{|s_k|}{|s_k| + \bar{s}_k + \varepsilon_s}, \qquad 0 \le e_s < w_s^{ad} \tag{3.11}$$

where $\varepsilon_s = 10^{-6}$. The sliding-mode driving term is introduced to reflect the direct demand of the current error for the control gain. When $|s_k| \ll \bar{s}_k$, $e_s \approx 0$, thereby avoiding excessive control under small errors; when $|s_k| \gg \bar{s}_k$, $e_s \to w_s^{\text{ad}}$, thus rapidly strengthening the control action. Moreover, the fractional structure guarantees that this term is bounded and monotonic, preventing the gain from increasing without a bound.

$$e_r = w_r^{ad} \frac{\bar{r}_k}{|r_k| + \bar{r}_k + \varepsilon_r}, \qquad 0 < e_r \le w_r^{ad} \tag{3.12}$$

where $\varepsilon_r = 10^{-6}$. The distance suppression term serves as an adaptive suppression and regularization mechanism. When r_k is small, the suppression effect is strong, preventing overly aggressive control; when r_k is large, the suppression effect is automatically weakened, thereby releasing control freedom. This mechanism implies that gain regulation is driven not only by the error but is also constrained by the overall system scale or distance, which improves stability and safety.

By jointly considering the three excitation terms, the total excitation e is given by

$$e = e_t + e_s - e_r. \tag{3.13}$$

The total excitation is mapped to (0,1) through a hyperbolic tangent function to obtain the adaptive gain $g(t, s, r)$

$$g(t, s, r) = \frac{1}{2}(1 + tanh(e)). \tag{3.14}$$

Therefore, by combining the adaptive gain in Eq (3.14) with the reaching law in Eq (3.3), a novel adaptive double-power reaching law is constructed, as given in Eq (3.15)

$$\dot{s}_1 = \left[-l_1 |s_1|^{p_1} \operatorname{sgn}(s_1) - l_2 |s_1|^{p_2} \operatorname{sgn}(s_1)\right] g(t, s_1, x_1) \tag{3.15}$$

$$p_1 = \frac{n_1 + 1}{2} + \frac{n_1 - 1}{2} \operatorname{sgn}(|s_1| - 1) \tag{3.16}$$

$$p_2 = \frac{n_2 + 1}{2} + \frac{1 - n_2}{2} \operatorname{sgn}(|s_1| - 1), \tag{3.17}$$

where $l_1 > 0$, $l_2 > 0$, $n_1 > 1$, $\frac{1}{2} < n_2 < 1$.

From Eqs (2.5) and (3.2), one obtains

$$a_{Mr} = -\dot{s}_1 + r\,x_4^2 + r\,x_6^2\cos^2(\theta_L)\,. \tag{3.18}$$

To avoid the range unreachability caused by a deceleration-based guidance law and to prevent an excessively long flight time, a_{Mr} is not subjected to deceleration control during the initial guidance stage so that the missile delivering a deployable sonar device can approach the target at high speed. After a certain time instant t_k, in order to achieve deceleration, a_{Mr} is then regulated. Therefore, a two-phase deceleration guidance design is adopted along the LOS direction. However, the two-phase deceleration scheme may require a relatively large acceleration command in the latter phase, which can induce an acceleration jump at t_k and impose considerable stress on the onboard actuators. Accordingly, a smoothly varying function $f_s(t)$ is further designed to switch the LOS guidance law in a bumpless manner. Specifically, the LOS deceleration sliding mode guidance law is given by

$$a_{Mr} = \begin{cases} 0, & t < t_k, \\ f_s(t)\left\{-\dot{s}_1 + rx_4^2 + rx_6^2\cos^2(\theta_L)\right\}, & t \geq t_k, \end{cases} \tag{3.19}$$

where

$$f_s(t) = 1 - e^{-k_s(t-t_k)}, \qquad k_s > 0,\ t_k > 0. \tag{3.20}$$

Theorem 1. *For the LOS subsystem Eq* (2.5)*, by selecting Eq* (3.1) *as the sliding surface and Eq* (3.15) *as the reaching law, the sliding variable of this subsystem converges to 0 within a fixed time, and* x_2 *achieves fixed-time convergence as well.*

Proof. From Eq (3.10), since $t \geq 0$, it follows that $e_t \geq -w_t t_{ref}$. From Eq (3.11), because both the numerator and the denominator in the expression of e_s are non-negative, one has $e_s \geq 0$. In addition, from Eq (3.9) together with $tanh(d_r) \in (-1, 1)$, it follows that $0 < w_r^a d < 1.3w_r$. Then, from Eq (3.12), one obtains $0 < e_r < w_r^a d < 1.3w_r$. Therefore, we have

$$e = e_t + e_s - e_r \geq -w_t t_{ref} - 1.3w_r = e_{min}.$$

Thus, from Eq (3.14), it follows that

$$g(t, s_1, x_1) = 1/2\,(1 + tanh(e)) \geq 1/2\,(1 + tanh(e_{min})) = g_{min} > 0.$$

Therefore, g_{min} is a uniform positive constant lower bound that is independent of the time and states. The derived lower bound is conservative, and it is introduced only for the theoretical proof of fixed-time convergence; in simulations, the observed practical convergence is much faster.

Choose the Lyapunov function as follows

$$V = \frac{1}{2}s_1^2. \tag{3.21}$$

Then

$$\dot{V} = s_1\dot{s}_1 = -g(t, s_1, R)\left(l_1|s_1|^{p_1+1} + l_2|s_1|^{p_2+1}\right) \leq 0.$$

Moreover, when $s_1 \neq 0$ and $g(t, s_1, R) \geq g_{min} > 0$, one has $\dot{V} < 0$. Hence, $s_1(t)$ exhibits a monotonic "energy decrease" and can only stop at $s_1 = 0$, implying $s_1 \to 0$. Therefore, $|s_1|$ is differentiable for $s_1 \neq 0$.

When $|s_1| > 1$, $sgn(|s_1| - 1) = 1$, and thus $p_1 = n_1 > 1$ and $p_2 = 1$. In this case, by combining with Eq (3.15), the time derivative of the absolute value of s_1 satisfies

$$|\dot{s_1}| = \text{sgn}(s_1)\dot{s}_1 = -g(t, s_1, x_1)\,(l_1|s_1|^{n_1} + l_2|s_1|) \leq -g_{\min}\,(l_1|s_1|^{n_1} + l_2|s_1|) \leq -g_{\min} l_1 |s_1|^{n_1}.$$

Let $z(t) = |s_1(t)|$. Then $\dot{z} \leq -g_{min} l_1 z^{n_1} < 0$. Since $z(t)$ is monotonically decreasing, $dz < 0$, and the variables can be separated to yield

$$dt = \frac{dz}{\dot{z}} \leq \frac{dz}{-g_{min} l_1 z^{n_1}}.$$

Integrating both sides yields an upper bound on the time required for $z(0)$ to reach $z(t) = |s_1(t)| = 1$:

$$T_{11} = \int_0^{T_{11}} dt \leq \int_{z(0)}^{1} -\frac{dz}{g_{min} l_1 z^{n_1}} = \frac{1 - z(0)^{1-n_1}}{g_{min} l_1 (n_1 - 1)}.$$

Since $|s_1| > 1$, one has $z(0) = |s_1(0)| > 1$. Moreover, because $1 - n_1 < 0$, it follows that $z(0)^{1-n_1} < 1$, and hence

$$T_{11} \leq \frac{1}{g_{min} l_1 (n_1 - 1)}.$$

When $|s_1| \leq 1$, $sgn(|s_1| - 1) = -1$, and thus $p_1 = 1$ and $p_2 = n_2 \in (0, 1)$. In this case, in combination with Eq (3.15), the time derivative of the absolute value of s_1 satisfies

$$|\dot{s_1}| = \text{sgn}(s_1)\dot{s}_1 = -g(t, s_1, x_1)\,(l_1|s_1| + l_2|s_1|^{n_2}) \leq -g_{\min}\,(l_1|s_1| + l_2|s_1|^{n_2}) \leq -g_{\min} l_2 |s_1|^{n_2}.$$

Similarly, integrating $|\dot{s_1}| \leq -g_{min} l_2 |s_1|^{n_2}$ yields an upper bound on the time required for $|s_1(t)|$ to decrease from 1 to 0

$$T_{12} \leq \frac{1}{g_{min} l_2 (1 - n_2)}.$$

Therefore, the convergence time of the sliding variable for this subsystem admits an upper bound T_1 (fixed time) that is independent of the initial conditions:

$$T_{11} + T_{12} \leq \frac{1}{g_{min} l_1 (n_1 - 1)} + \frac{1}{g_{min} l_2 (1 - n_2)} = T_1. \tag{3.22}$$

In combination with Eq (3.1), it follows that

$$\lim_{t \to T_1} x_2(t) = \lim_{t \to T_1} (v_d + s_1) = v_d. \tag{3.23}$$

Therefore, x_2 achieves state convergence within T_1. This completes the proof of Theorem 1. □

3.2. Design of the LOS normal and lateral impact angle constrained sliding mode guidance law

To realize impact angle-constrained guidance in the LOS normal direction, the sliding surface [41–43] is selected as follows:

$$s_2 = x_3 + k_1 |x_3|^{q_1} \text{sgn}(x_3) + k_2 |x_4|^{q_2} \text{sgn}(x_4), \tag{3.24}$$

where $k_1 > 0$, $k_2 > 0$, $q_1 > 1$, $q_2 > 1$, $q_1 > q_2$. The corresponding reaching law also incorporates the adaptive gain designed in this paper, as follows:

$$\dot{s}_2 = \left[-l_1|s_2|^{p_3}\,\mathrm{sgn}(s_2) - l_2|s_2|^{p_4}\,\mathrm{sgn}(s_2)\right] g(t, s_2, x_1), \tag{3.25}$$

where

$$p_3 = \frac{n_1+1}{2} + \frac{n_1-1}{2}\,\mathrm{sgn}\left(|s_2|-1\right) \tag{3.26}$$

$$p_4 = \frac{n_2+1}{2} + \frac{1-n_2}{2}\,\mathrm{sgn}\left(|s_2|-1\right). \tag{3.27}$$

Taking the time derivative of both sides of Eq (3.24) yields

$$\dot{s}_2 = \dot{x}_3 + k_1 q_1\,|x_3|^{q_1-1}\,\dot{x}_3 + k_2 q_2\,|x_4|^{q_2-1}\,\dot{x}_4.$$

From Eq (2.8), one has

$$\dot{x}_3 = x_4, \dot{x}_4 = -\frac{2x_2x_4}{x_1} - x_6^2 sin\theta_L cos\theta_L - \frac{a_{M\theta}}{x_1}.$$

Substituting into the expression above yields

$$\dot{s}_2 = x_4 + k_1 q_1\,|x_3|^{q_1-1}\,x_4 + k_2 q_2\,|x_4|^{q_2-1}\left(-\frac{2x_2x_4}{x_1} - x_6^2\sin\theta_L\cos\theta_L - \frac{a_{M\theta}}{x_1}\right).$$

Rearranging yields

$$a_{M\theta} = \frac{-x_1\dot{s}_2 + x_1x_4 + k_1q_1x_1|x_3|^{q_1-1}\cdot x_4}{k_2q_2|x_4|^{q_2-1}} - 2x_2x_4 - x_1x_6^2\sin\theta_L\cos\theta_L. \tag{3.28}$$

Eq (3.28) is an explicit closed-form expression obtained by algebraic manipulation under the condition $x_4 \neq 0$. When $x_4 \to 0$, the denominator term $|x_4|^{q_2-1}$ will approach zero, which makes this explicit inversion ill-posed in the vicinity of the singular point. It should be emphasized that the present work focuses on the theoretical design of the command-level three-dimensional guidance law and its convergence analysis. Practical implementation issues near $x_4 = 0$ can be handled using standard techniques such as regularization or piecewise implementation; this part will be further investigated in future work.

Theorem 2. *For the LOS normal subsystem Eq* (2.6)*, by selecting Eq* (3.24) *as the sliding surface and Eq* (3.25) *as the reaching law, the sliding variable of this subsystem converges to 0 within a fixed time, and x_3,x_4 converge to 0 within a fixed time as well.*

Proof. Since the reaching law of this subsystem has exactly the same structure as that in Theorem 1, it similarly follows that the convergence time of the sliding variable admits an upper bound T_2 (fixed time) that is independent of the initial conditions.

$$T_2 = \frac{1}{g_{min}l_1\,(n_1-1)} + \frac{1}{g_{min}l_2\,(1-n_2)}. \tag{3.29}$$

After the sliding surface is reached, $s_2 = 0$, yielding

$$k_2|x_4|^{q_2}\,\mathrm{sgn}(x_4) = -\left(x_3 + k_1|x_3|^{q_1}\,\mathrm{sgn}(x_3)\right). \tag{3.30}$$

By using the inverse of the mapping $y = |x|^{q_2}\,\mathrm{sgn}(x)$, i.e., $x = |y|^{q_2}\,\mathrm{sgn}(y)$, and combining it with Eq (3.30) and the system equation $\dot{x}_3 = x_4$, it follows that

$$\dot{x}_3 = -k_2^{1/q_2}\left|x_3 + k_1|x_3|^{q_1}\,\mathrm{sgn}(x_3)\right|^{1/q_2}\,\mathrm{sgn}(x_3 + k_1|x_3|^{q_1}\,\mathrm{sgn}(x_3)). \tag{3.31}$$

Note that $x_3 + k_1\,|x_3|^{q_1}\,sgn\,(x_3) = x_3(1 + k_1\,|x_3|^{q_1})$. Since $k_1 > 0$, it follows that $1 + k_1\,|x_3|^{q_1} > 0$, and thus $sgn\,(x_3 + k_1\,|x_3|^{q_1}\,sgn\,(x_3)) = sgn\,(x_3)$. Therefore, from Eq (3.31), one obtains

$$\dot{x}_3 = -k_2^{-1/q_2}\,|x_3 + k_1|\,x_3|^{q_1}\,sgn(x_3)|^{1/q_2}\,sgn\,(x_3)\,. \tag{3.32}$$

Choose the Lyapunov function as follows:

$$W = \frac{1}{2}x_3^2. \tag{3.33}$$

From Eqs (3.32) and (3.33), it follows that

$$\dot{W} = x_3\dot{x}_3 \le -k_2^{-1/q_2}\,|x_3|\,\left|x_3 + k_1|x_3|^{q_1}\,\mathrm{sgn}(x_3)\right|^{1/q_2} \le 0. \tag{3.34}$$

Therefore, W is monotonically decreasing. Let $\varepsilon = \frac{1}{2}k_1^{-2/(q_1-1)} > 0$. When $W > \varepsilon$, $k_1\,|x_3|^{q_1} > |x_3|$; when $W \le \varepsilon$, $k_1\,|x_3|^{q_1} \le |x_3|$.

When $W > \varepsilon$, $|x_3 + k_1|\,x_3|^{q_1}\,sgn(x_3)|^{1/q_2} \ge k_1\,|x_3|^{q_1}$. In combination with Eq (3.34), $\dot{W}$ satisfies

$$\dot{W} \le -k_1k_2^{-1/q_2}|x_3|^{1+q_1/q_2} = -c_2W^{\delta} \tag{3.35}$$

$$c_2 = k_1k_2^{-1/q_2} > 0$$

$$\delta = \frac{1 + q_1/q_2}{2} > 1.$$

From Eq (3.35), one obtains

$$W^{-\delta}\dot{W} \le -c_2.$$

Taking the time derivative of $W^{1-\delta}$ yields

$$\frac{d}{dt}\left(W^{1-\delta}\right) = (1-\delta)W^{-\delta}\dot{W} \ge (1-\delta)(-c_2) = (\delta-1)c_2 > 0. \tag{3.36}$$

Integrating both sides of Eq (3.36) yields

$$W\,(t)^{1-\delta} \ge W\,(0)^{1-\delta} + (\delta-1)\,c_2t.$$

Let $W\,(t_\varepsilon) = \varepsilon$, yielding

$$t_\varepsilon \le \frac{\varepsilon^{1-\delta} - W\,(0)^{1-\delta}}{(\delta-1)\,c_2}.$$

Since $1-\delta<0$, when $W(0)\to\infty$, one has $W(0)^{1-\delta}\to 0$. Hence, t_ε admits an upper bound

$$t_\varepsilon \le \frac{\varepsilon^{1-\delta}}{(\delta-1)\,c_2} = T_{31}. \tag{3.37}$$

When $W\le\varepsilon$, $|x_3+k_1|x_3|^{q_1}sgn(x_3)|^{1/q_2}\ge|x_3|$. In combination with Eq (3.34), $\dot{W}$ satisfies

$$\dot{W}\le -k_2^{-1/q_2}\,|x_3|^{1+1/q_2} = -c_1 W^{\gamma}$$

where

$$c_1 = k_2^{-1/q_2} > 0$$

$$\gamma = \frac{1+1/q_2}{2}\in(0.5,1).$$

According to Lemma 1, x_3 converges to 0 within T_{32}

$$T_{32} = \frac{\varepsilon^{1-\gamma}}{c_1\,(1-\gamma)}. \tag{3.38}$$

Therefore, for any initial value $W(0)\ge 0$, the total convergence time T_3 satisfies

$$T_3 = T_{31}+T_{32} = \frac{\varepsilon^{1-\delta}}{(\delta-1)\,c_2} + \frac{\varepsilon^{1-\gamma}}{c_1\,(1-\gamma)}. \tag{3.39}$$

The right-hand side of Eq (3.39) does not contain $W(0)$. Therefore, there is a constant T_3 independent of the initial conditions such that $W(t)=0$ for $t\ge T_3$, i.e., $x_3(t)=0$.

Furthermore, taking the absolute value on both sides of Eq (3.30) yields

$$k_2\,|x_4|^{q_2} = |x_3|\,(1+k_1\,|x_3|^{q_1-1}),$$

i.e.,

$$|x_4| = k_2^{-1/q_2}\,|x_3|^{1/q_2}\left(1+k_1\,|x_3|^{q_1-1}\right)^{1/q_2}.$$

It follows that, as $x_3\to 0$, one must have $x_4\to 0$. Therefore, (x_3,x_4) converges to (0,0) within a fixed time. This completes the proof of Theorem 2. □

To realize impact angle-constrained guidance in the LOS lateral direction, the sliding surface is selected as follows:

$$s_3 = x_5 + k_1|x_5|^{q_1}\,\mathrm{sgn}(x_5) + k_2|x_6|^{q_2}\,\mathrm{sgn}(x_6). \tag{3.40}$$

The corresponding reaching law is given as follows:

$$\dot{s}_3 = \left[-l_1|s_3|^{p_5}\,\mathrm{sgn}(s_3) - l_2|s_3|^{p_6}\,\mathrm{sgn}(s_3)\right] g(t,s_3,x_1), \tag{3.41}$$

where

$$p_5 = \frac{n_1+1}{2} + \frac{n_1-1}{2}\,\mathrm{sgn}\left(|s_3|-1\right) \tag{3.42}$$

$$p_6 = \frac{n_2+1}{2} + \frac{1-n_2}{2}\,\mathrm{sgn}\left(|s_3|-1\right). \tag{3.43}$$

Taking the time derivative of both sides of Eq (3.40) and, in combination with Eq (2.8), yields the LOS lateral guidance law

$$a_{M\phi} = \frac{x_1\cos\theta_L\left(\dot{s}_3 - x_6 - k_1 q_1|x_5|^{q_1-1}\cdot x_6\right)}{k_2 q_2|x_6|^{q_2-1}} + 2x_2x_6\cos\theta_L - 2x_1x_4x_6\sin\theta_L. \tag{3.44}$$

Theorem 3. *For the LOS lateral subsystem Eq* (2.7)*, by selecting Eq* (3.40) *as the sliding surface and Eq* (3.41) *as the reaching law, the sliding variable of this subsystem converges to 0 within a fixed time, and x_5,x_6 converge to 0 within a fixed time as well.*

From Eqs (2.7) and (2.8), it follows that

$$\dot{x}_5 = x_6, \dot{x}_6 = -\frac{2x_2x_6}{x_1} + 2x_4x_6\tan\theta_L + \frac{a_{M\phi}}{x_1\cos\theta_L}.$$

Note that this subsystem contains $\cos\theta_L$ and $\tan\theta_L$ terms; therefore, its regularity needs to be further clarified. Since the water-entry angle constraint considered in this paper and the initial engagement geometry correspond to a bounded LOS elevation angle range, and the desired LOS elevation angle does not correspond to a vertical limit case, θ_L always evolves within a regular feasible interval away from singularities.

Assume that there is a constant $\varepsilon_\theta > 0$ during the guidance process such that

$$|\theta_L(t)| \le \frac{\pi}{2} - \varepsilon_\theta.$$

One then has

$$\cos\theta_L(t) \ge \cos\left(\frac{\pi}{2} - \varepsilon_\theta\right) > 0, |\tan\theta_L(t)| \le \tan\left(\frac{\pi}{2} - \varepsilon_\theta\right) < \infty.$$

Therefore, the lateral subsystem is well-defined over the entire guidance interval. Furthermore, by substituting Eq (3.44) into the equation above, the two coupling terms $-\frac{2x_2x_6}{x_1}$ and $2x_4x_6tan\theta_L$ are exactly compensated, and the closed-loop dynamics with respect to (x_5, x_6) can be reduced to the same standard form as (x_3, x_4) in Theorem 2. Therefore, following an analysis procedure similar to that of Theorem 2, one can conclude that the sliding variable s_3 converges to 0 within a fixed time, and the states x_5, x_6 converge to 0 within a fixed time as well.

4. Simulation tests

To rapidly and safely deliver the deployable sonar device to the target sea area, the proposed adaptive two-phase guidance law for the missile delivering a deployable sonar device divides the overall guidance process into two phases. In the first phase, the missile rapidly approaches the target, whereas in the second phase, the missile–target relative velocity is constrained along the LOS direction. As a result, the missile can reach the target stably within a shorter time, with a smaller water-entry angle and a lower impact velocity. To demonstrate the superiority of the proposed approach, this chapter conducts simulation tests for full-phase deceleration guidance, two-phase deceleration guidance, and adaptive two-phase deceleration guidance, as well as comparisons with other guidance laws.

In the subsequent simulations, the initial position of the missile delivering a deployable sonar device is set to (0,0,0) m, and the position of the stationary target is set to (11350,0,4199.2) m. The initial state of the missile is set as V_M = 800 m/s, $\vartheta_M = 15°$, and $\psi_M = 0°$. The desired impact velocity is set as V_d = 300 m/s. The acceleration upper limit is set to 30×g. The parameter settings of the proposed guidance law are listed in Table 1.

Table 1. Guidance law parameter settings.

Parameter	Value	Parameter	Value	Parameter	Value
l_1	0.5	k_s	0.1	q_1	5/3
l_2	0.5	t_k	10	q_2	11/9
n_1	9/7	k_1	2.1		
n_2	7/9	k_2	6.1		

4.1. Full-phase guidance for the missile delivering a deployable sonar device

This section considers a baseline simulation in which the adaptive gain $g(t, s, r)$ designed in this paper is not used and the two-phase deceleration scheme is not applied, serving as a reference for the subsequent simulation cases. For the three subsystems along the LOS direction, the LOS normal direction, and the LOS lateral direction, the sliding surfaces are given by Eq (3.1), Eq (3.24), and Eq (3.40), respectively, and the reaching laws in all three subsystems adopt the double-power reaching law in Eq (3.3). The corresponding guidance laws are given by Eq (3.18), Eq (3.28), and Eq (3.44), respectively. Figure 2 presents the simulation results of this guidance law under different desired water-entry angles. The four curves correspond to $\theta_{Ld} = -25^\circ$, -20°, -15°, and -10°, respectively, while the corresponding values of ϕ_{Ld} are all -30°.

As shown in Figure 2(a),(b), under four different desired impact angle constraints, the missile delivering a deployable sonar device can reach the target in all cases, and the flight time is nearly identical. As shown in Figure 2(c), to achieve the desired impact angles, the missile needs to climb to a certain altitude first. Consequently, V_M increases slightly during the initial stage of guidance, and then decreases rapidly, converging and remaining stable at around 10 s. The missile–target relative velocity converges and remains stable in an even shorter time. However, converging too early to the desired missile–target relative velocity (i.e., decelerating too early) increases the total flight time, thereby delaying the execution of the sonar detection mission. From Figure 2(d)–(g), the LOS elevation angle and LOS azimuth angle of each case converge to their respective desired values at around 10 s and remain stable, while the LOS angular rates converge to 0. Figures 2(h)–(j) show the acceleration histories along the LOS direction, the LOS normal direction, and the LOS lateral direction. Acceleration saturation occurs at the very beginning in all three directions; after a few seconds, the accelerations in all three directions vary sharply and change sign, and then converge to 0. Although no abrupt jumps in the acceleration command are observed, the early-stage acceleration saturation and sharp variations still impose considerable stress on the onboard actuators. Table 2 summarizes the simulation results of full-phase deceleration guidance. Under different desired impact angles, the miss distance is within 1 m in all cases, and the missile–target relative velocity error, the LOS elevation angle error, and the LOS azimuth angle error are all nearly zero, while the flight time is approximately 39.26 s in all cases.

Overall, although the guidance law in this section can accurately reach the target while satisfying both the impact velocity and impact angle constraints, it is necessary to further optimize the guidance law to avoid an excessively long flight time and to alleviate the load on the onboard actuators.

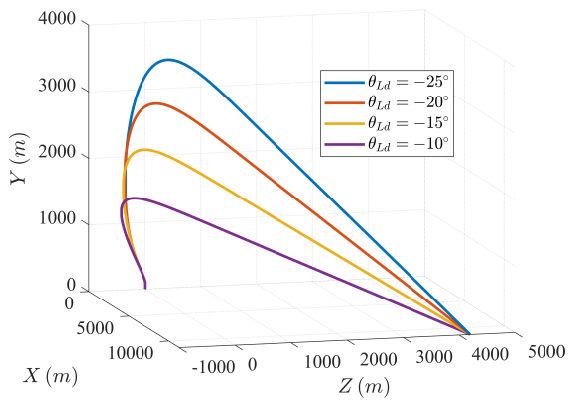

(a) Delivery trajectory

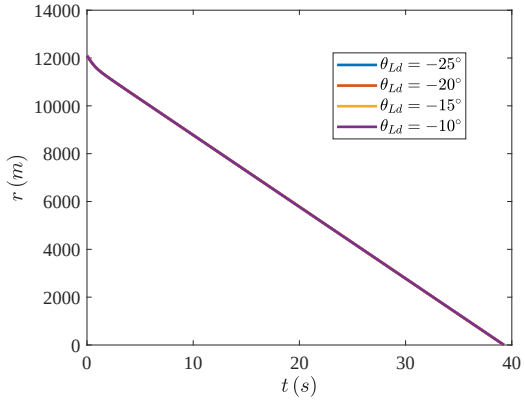

(b) Missile–target distance and remaining flight time

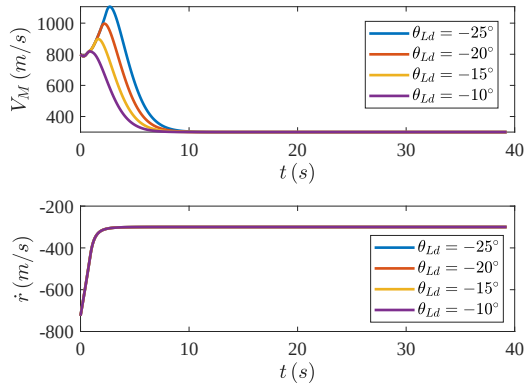

(c) Missile velocity and missile–target relative velocity

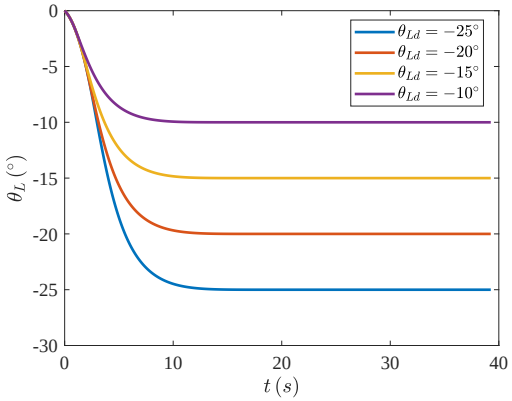

(d) LOS elevation angle

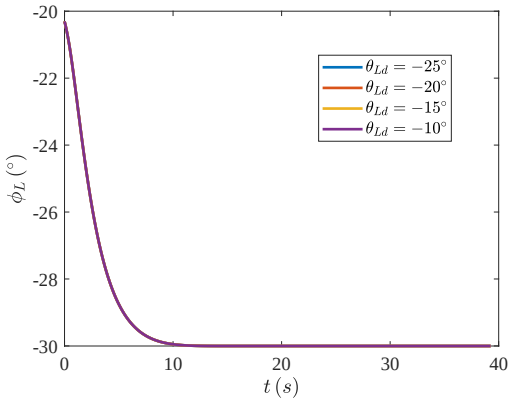

(e) LOS azimuth angle

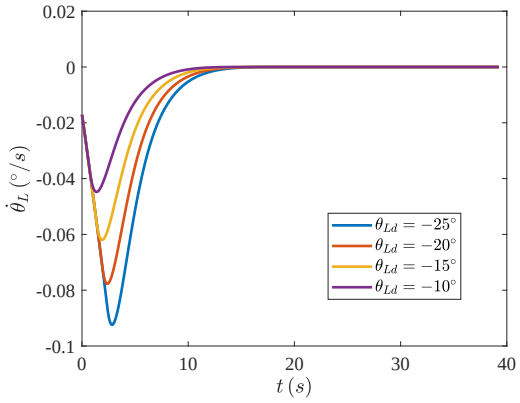

(f) LOS elevation angular rate

Figure 2. Full-phase guidance for the missile delivering a deployable sonar device.

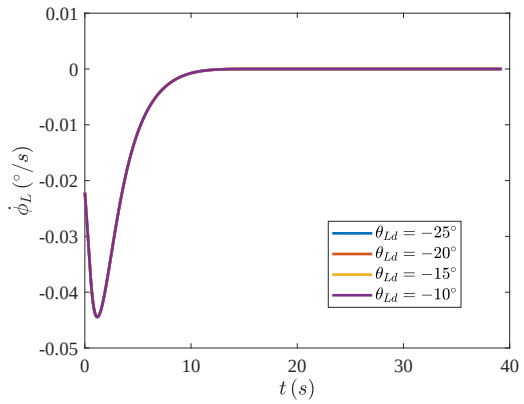

(g) LOS azimuth angular rate

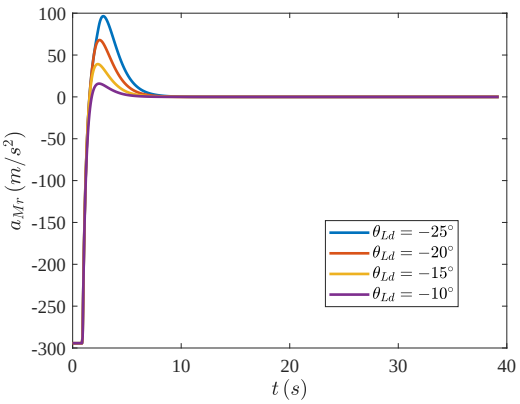

(h) LOS acceleration

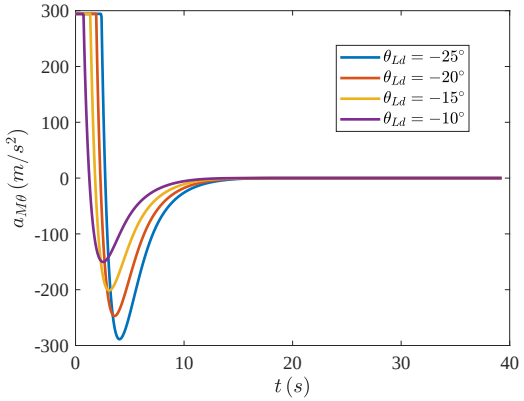

(i) LOS normal acceleration

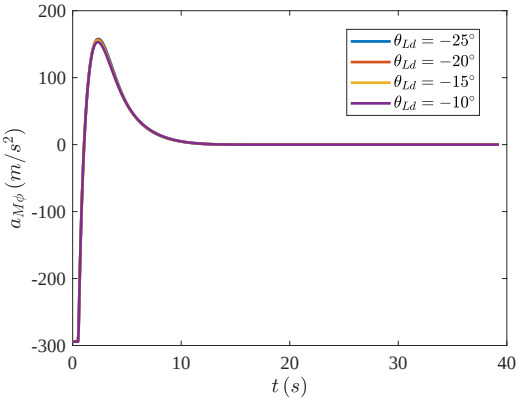

(j) LOS lateral acceleration

Figure 2. Full-phase guidance for the missile delivering a deployable sonar device.

Table 2. Simulation results of full-phase guidance.

Parameter	Value	Parameter	Value	Parameter	Value
$\theta_{Ld}(^\circ)$	Miss distance (m)	$\dot{r}$ error (m/s)	θ_L error (°)	ϕ_L error (°)	Flight time (s)
-25	0.80534	1E-15	3.0615E-11	-1.6228E-11	39.26
-20	0.74345	-5.6843E-14	4.1525E-11	1.5268E-13	39.26
-15	0.98888	-5.6843E-14	2.773E-11	-3.5682E-11	39.259
-10	0.9246	1E-15	-2.7132E-11	-5.8043E-11	39.259

4.2. Two-phase guidance for the missile delivering a deployable sonar device

To highlight the advantage of two-phase deceleration, the simulation in this section also does not consider the adaptive gain $g(t,s,r)$ designed in this paper. However, the guidance law along the LOS direction is implemented in two phases: Before 10 s, a_{Mr} is set to 0; starting from 10 s, the missile–target relative velocity is constrained, and a_{Mr} is further modified by using the smoothly

varying function designed in this paper. For the three subsystems along the LOS direction, the LOS normal direction, and the LOS lateral direction, the sliding surfaces are given by Eq (3.1), Eq (3.24), and Eq (3.40), respectively, and the reaching laws in all three subsystems adopt the double-power reaching law in Eq (3.3). The corresponding guidance laws are given by Eq (3.19), Eq (3.28), and Eq (3.44), respectively. Figure 3 presents the simulation results under different desired water-entry angles. The four curves correspond to $\theta_{Ld} = -25^\circ$, -20°, -15°, and -10°, respectively, while the corresponding ϕ_{Ld} are all -30°.

As shown in Figure 3(a)–(g), the guidance law in this section can also drive the impact velocity and impact angles of each missile to converge to the desired values and remain stable, and the target is accurately hit in all cases. Compared with the simulation results in Section 4.1, however, both the convergence time of the missile–target relative velocity and the total flight time change. As shown in Figure 3(c), V_M and the missile–target relative velocity exhibit a staircase-like profile: They first converge and stabilize at a constant value at around 5 s, and then gradually converge to the desired velocity from 10 s onward. This staircase-like behavior allows the missile to maintain a relatively high missile–target relative velocity during the initial guidance stage, thereby approaching the target rapidly and reducing the total flight time. As shown in Figure 3(h), after introducing the smoothly varying function in Eq (3.20), the variations of a_{Mr} for all four cases remain smooth when the missile–target relative velocity constraint is activated at 10 s, and no abrupt jumps in the acceleration command are observed, which is consistent with engineering requirements. If a_{Mr} is not modified by the smoothly varying function, as given in Eq (4.1), the corresponding simulation results are shown in Figure 4(a). In this case, a_{Mr} exhibits a jump at 10 s and acceleration saturation occurs, imposing considerable stress on the onboard actuators. Therefore, the smoothly varying function designed for a_{Mr} in this paper is necessary.

$$a_{Mr} = \begin{cases} 0, & t < t_k, \\ -\dot{s}_1 + rx_4^2 + rx_6^2 \cos^2(\theta_L), & t \geq t_k. \end{cases} \tag{4.1}$$

As shown in Figure 3(i),(j), acceleration saturation still occurs in the LOS normal and LOS lateral channels during the initial guidance stage. Table 3 summarizes the simulation results of the guidance law in this section. Compared with Table 2, the total flight times are 32.918 s, 30.398 s, 28.216 s, and 26.413 s, respectively, representing reductions of at least 6.342 s and up to 12.828 s. Therefore, the two-phase deceleration guidance achieves a significant reduction in flight time compared with the full-phase deceleration guidance, thereby ensuring the mission efficiency of sonar detection. However, to further enhance the stability of the guidance process, it is necessary to optimize the guidance law by incorporating the adaptive gain designed in this paper.

Table 3. Simulation results of two-phase guidance (without adaptive term).

Parameter	Value	Parameter	Value	Parameter	Value
$\theta_{Ld}(^\circ)$	Miss distance (m)	$\dot{r}$ error (m/s)	θ_L error (°)	ϕ_L error (°)	Flight time (s)
-25	0.702	5.6843E-14	1.7071E-11	4.5212E-11	32.918
-20	0.72085	5.6843E-14	3.5479E-11	1.96E-11	30.398
-15	0.93715	1E-15	2.2266E-14	-1.1993E-10	28.216
-10	0.90245	-4.1892E-4	-2.7132E-11	-5.8043E-11	26.413

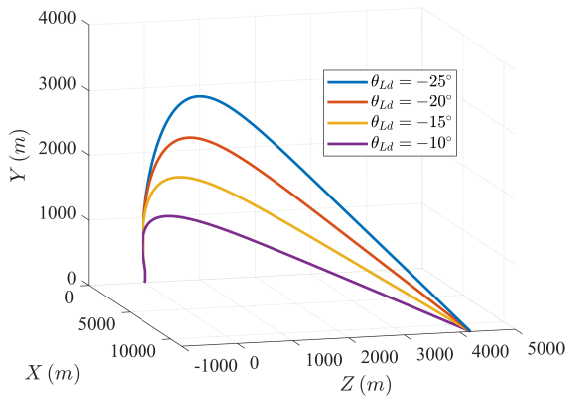

(a) Delivery trajectory

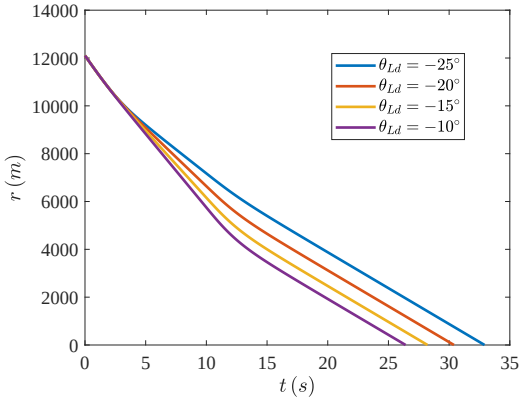

(b) Missile–target distance and remaining flight time

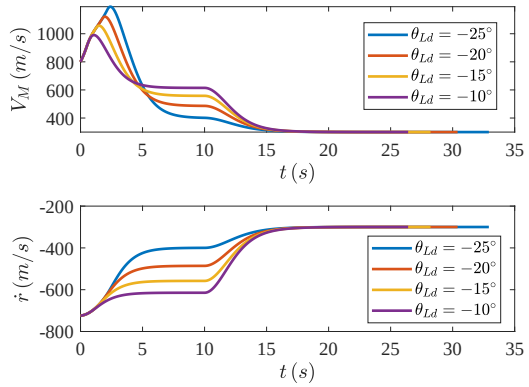

(c) Missile velocity and missile–target relative velocity

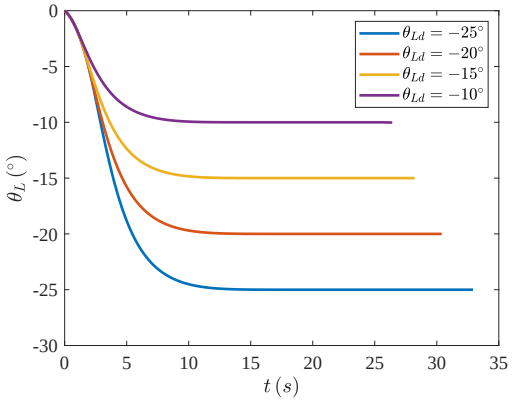

(d) LOS elevation angle

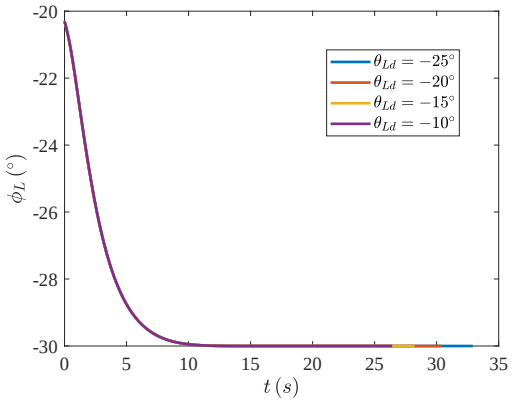

(e) LOS azimuth angle

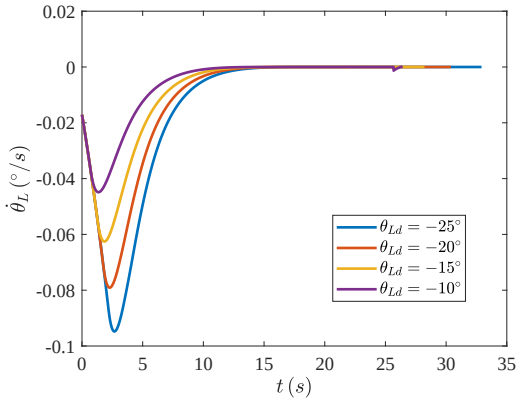

(f) LOS elevation angular rate

Figure 3. Two-phase guidance for the missile delivering a deployable sonar device.

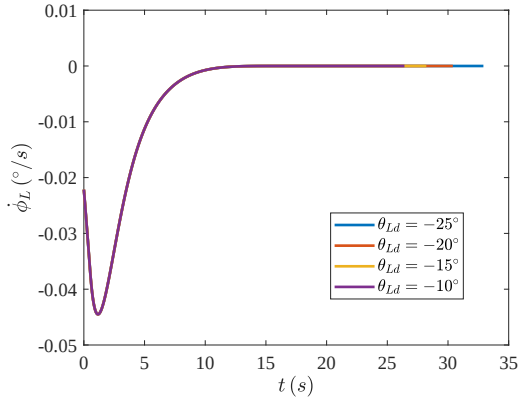

(g) LOS azimuth angular rate

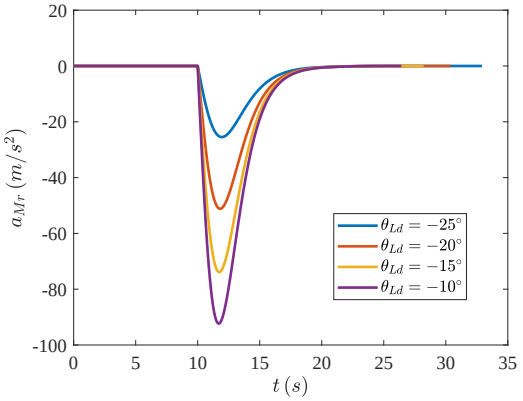

(h) LOS acceleration

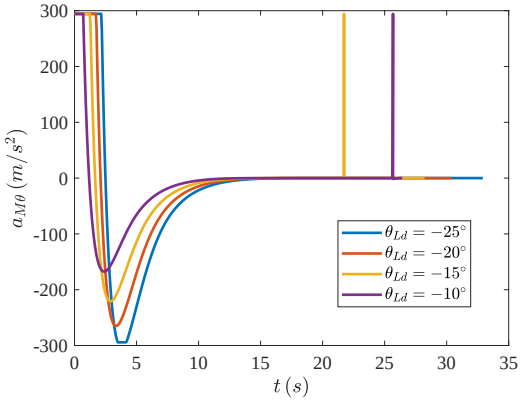

(i) LOS normal acceleration

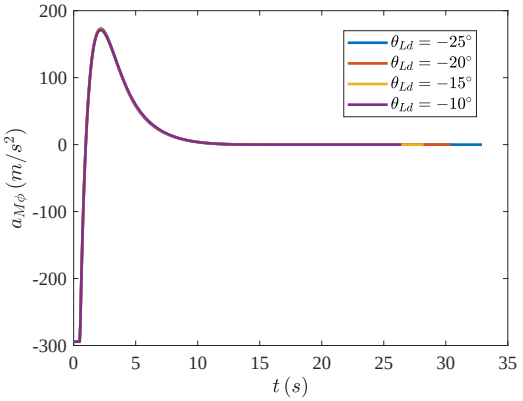

(j) LOS lateral acceleration

Figure 3. Two-phase guidance for the missile delivering a deployable sonar device.

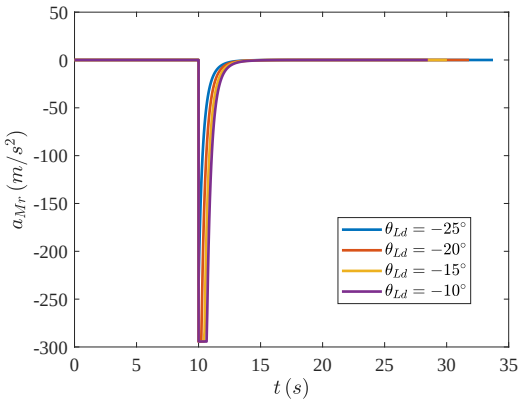

(a) Without using a smoothly varying function

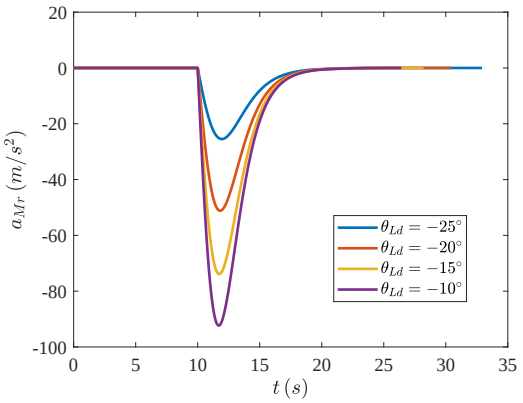

(b) Using a smoothly varying function

Figure 4. Effect of using a smoothly varying function on the LOS acceleration.

4.3. Adaptive two-phase guidance for the missile delivering a deployable sonar device

To verify the advantage of the adaptive gain designed for the reaching law in this paper, the simulation in this section adopts the proposed three-dimensional adaptive guidance law for the missile delivering a deployable sonar device. For the three subsystems along the LOS direction, the LOS normal direction, and the LOS lateral direction, the sliding surfaces are given by Eq (3.1), Eq (3.24), and Eq (3.40), respectively; the reaching laws are given by Eq (3.15), Eq (3.25), and Eq (3.41), respectively; and the corresponding guidance laws are given by Eq (3.19), Eq (3.28), and Eq (3.44), respectively. Figure 5 presents the simulation results under different desired water-entry angles. The four curves correspond to $\theta_{Ld} = -25^\circ$, -20°, -15°, and -10°, respectively, while the corresponding values of ϕ_{Ld} are all -30°.

As shown in Figure 5(a)–(g), the guidance law developed in this paper can drive the impact velocity and impact angles of each missile to converge to the desired values and remain stable, and the target is accurately hit in all cases. As shown in Figure 5(a),(b), the missile delivering a deployable sonar device can accurately reach the target under different desired impact angles. The overall trajectory is smooth and stable: In the early guidance stage, the missile flies toward the target along a shorter path, and in the later stage, it adjusts the impact angles, thereby reducing the total flight time to within 25 s in all cases. As shown in Figure 5(c), V_M increases slightly at around 10 s to allow the missile to climb to a certain altitude and adjust the impact angles. After 10 s, V_M and the missile–target relative velocity gradually converge to the desired velocity, and the entire process is smooth without chattering. Maintaining a relatively high velocity in the early guidance stage facilitates rapid target approach and helps reduce the total flight time. As shown in Figure 5(d)–(g), the LOS elevation angle and line-of-sight azimuth angle in each case converge to their respective desired values and remain stable, while the LOS angular rates converge to 0. As shown in Figure 5(h)–(j), the acceleration histories along the LOS direction, the LOS normal direction, and the LOS lateral direction are smooth for most of the time. The small jumps of $a_{M\theta}$ and $a_{M\phi}$ at 10 s are expected and acceptable. More importantly, compared with Figure 2(i),(j), and Figure 3(i),(j), no acceleration saturation is observed for $a_{M\theta}$ and $a_{M\phi}$ in the simulations of this section, which substantially reduces the load on the onboard actuators and better satisfies engineering requirements. Table 4 summarizes the simulation results of the proposed guidance law, where the miss distances are all within 1 m, indicating accurate target interception. Compared with Tables 2 and 3, the missile–target relative velocity error, the LOS elevation angle error, and the LOS azimuth angle error in this case are several orders of magnitude larger; nevertheless, they remain at the order of E-02 or lower, meeting the requirements of the impact velocity constraint and impact angle constraint, and thus achieving the guidance objective. More importantly, the total flight time is further reduced to 23.732 s, 23.402 s, 23.165 s, and 23.022 s, respectively. Compared with Table 1, the flight time is reduced by approximately 16 s, i.e., a reduction of about 40%, which significantly improves the mission efficiency of delivering the deployable sonar device.

Overall, by comparing Figures 2, 3, and 5, the proposed guidance law substantially shortens the deployment time of the deployable sonar device relative to the guidance laws used in Sections 4.1 and 4.2, thereby noticeably improving mission efficiency. Meanwhile, no acceleration saturation or chattering is observed along the LOS, LOS normal, and LOS lateral directions, which greatly alleviates the burden on the onboard actuators.

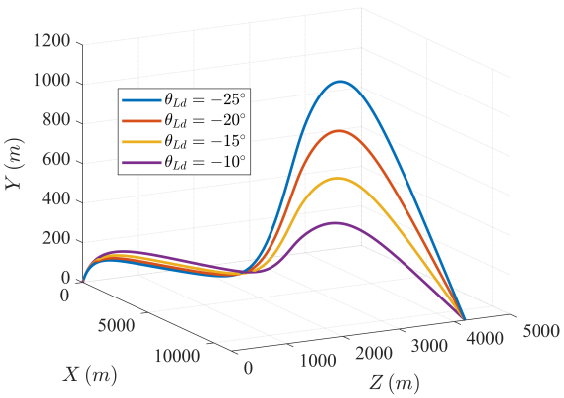

(a) Delivery trajectory

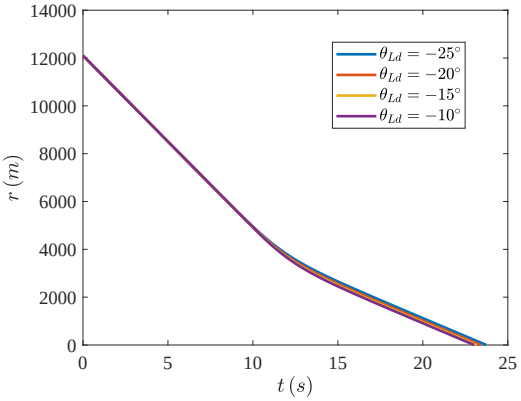

(b) Missile–target distance and remaining flight time

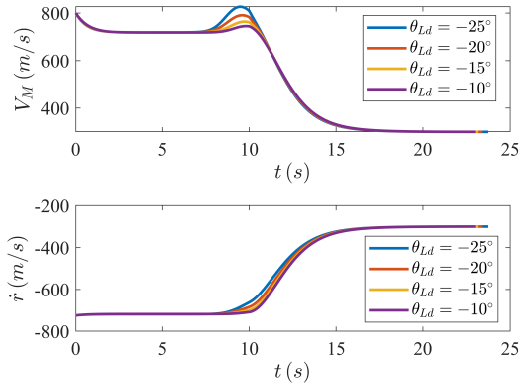

(c) Missile velocity and missile–target relative velocity

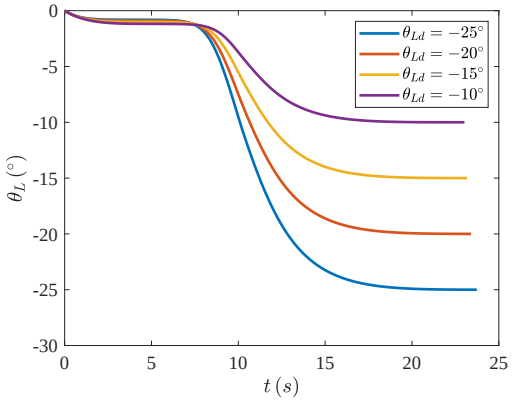

(d) LOS elevation angle

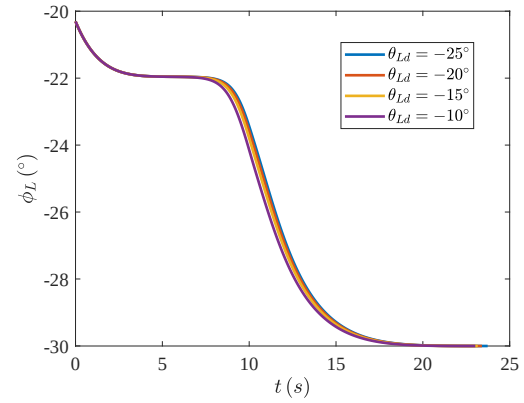

(e) LOS azimuth angle

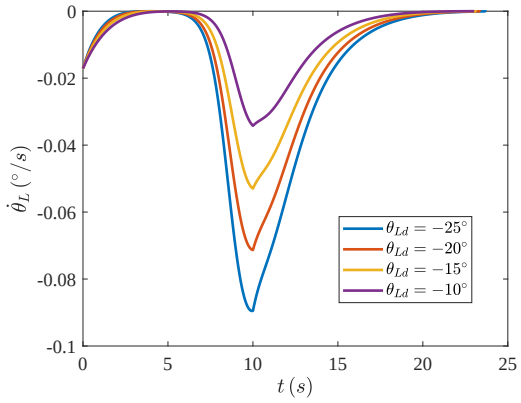

(f) LOS elevation angular rate

Figure 5. Adaptive two-phase guidance for the missile delivering a deployable sonar device.

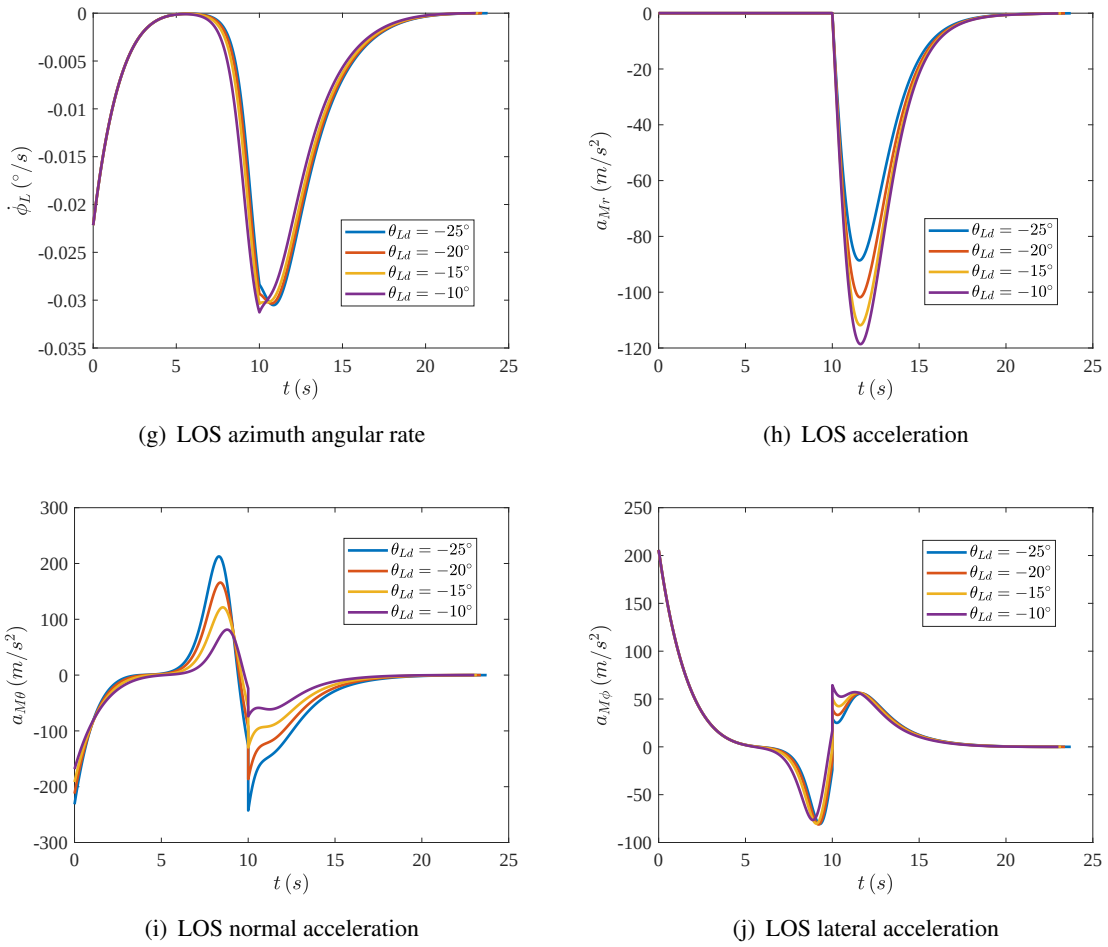

(g) LOS azimuth angular rate

(h) LOS acceleration

(i) LOS normal acceleration

(j) LOS lateral acceleration

Figure 5. Adaptive two-phase guidance for the missile delivering a deployable sonar device.

Table 4. Simulation results of adaptive two-phase guidance.

Parameter	Value	Parameter	Value	Parameter	Value
$\theta_{Ld}(^\circ)$	Miss distance (m)	$\dot{r}$ error (m/s)	θ_L error ($^\circ$)	ϕ_L error ($^\circ$)	Flight time (s)
-25	0.9557	-3.5301E-02	1.7685E-03	5.4063E-05	23.732
-20	0.75391	-5.6521E-02	1.4291E-03	1.0412E-04	23.402
-15	0.94602	7.7025E-02	7.7478E-04	1.3928E-04	23.165
-10	0.84947	-9.2314E-02	1.7177E-04	1.2339E-04	23.022

4.4. Comparison with other guidance laws

To demonstrate the advantages of the proposed three-dimensional adaptive guidance law for the missile delivering a deployable sonar device after improving the double-power reaching law, this section compares the proposed guidance law with other guidance laws under identical test conditions. It should be noted that the primary purpose of our simulations is not to establish a unified benchmark

against all existing guidance laws, but rather, under the specific mission background of delivering a deployable sonar device by missile, to validate the concrete roles of the two-phase deceleration mechanism and the adaptive gain design. Since the existing three-dimensional guidance laws with terminal angle and/or terminal velocity constraints differ markedly from this work in terms of their modeling foundations, mission requirements, constraint formulations, and parameter settings, a direct side-by-side comparison would be difficult to ensure fairness and task relevance. Meanwhile, the main advantage of the proposed method is not to merely pursue extreme terminal accuracy, but to further shorten the flight time, reduce early-stage acceleration peaks, and alleviate the early control burden on the onboard actuators, while the terminal velocity and angle errors already meet the mission requirements.

References [46, 47] present nonsingular sliding mode guidance laws with angle constraints, as shown in Figure 6. For L2 and L3, the reaching laws are adopted from these two references, respectively, with the reaching law parameters kept consistent with the original papers, while the sliding surfaces are the same as those used in this paper. Meanwhile, for L2 and L3, the expression of a_{Mr} is modified to follow the same two-phase design as in this paper, and the smoothly varying function in Eq (3.20) is also applied. L1 denotes the proposed three-dimensional adaptive guidance law for the missile delivering a deployable sonar device, which is identical to that in Section 4.3. L4 is the same guidance law as that used in Section 4.1, which adopts the double-power reaching law; L4 is included here to more directly illustrate the advantage of the proposed guidance law under the same test conditions. In this simulation, θ_{Ld} for L1–L4 is set to -20°, and ϕ_{Ld} is set to -30° for all cases.

It should be noted that the controller design and Lyapunov-based convergence analysis in Section 3 are established in a continuous-time framework, whereas the simulations in this section are implemented digitally with a fixed guidance cycle $\Delta t = 0.001$ s. At each update instant, the sampled state is used to compute the sliding variables, then the adaptive historical averages and gain are updated according to Eqs (3.4)–(3.14), and finally the corresponding guidance commands are generated from Eqs (3.19), (3.28), and (3.44). In addition, all compared laws in this section are tested under the same engagement scenario, initial conditions, target setting, terminal constraints, acceleration limits, numerical step size, and evaluation metrics. The purpose of this comparison is to examine the influence of different reaching law or adaptive gain designs under the same mission background.

As shown in Figure 6(a), the trajectories of L2–L4 are similar: They climb early to adjust the LOS angles during the initial guidance stage. In contrast, the proposed L1 first flies toward the target along a shorter path in the early guidance stage and adjusts the impact angles when it is close to intercepting the target, which helps shorten the total flight time. Consequently, the flight path of L1 is clearly shorter than those of L2–L4. As shown in Figure 6(b), the proposed guidance law achieves accurate target interception in a shorter time. As shown in Figure 6(c), compared with L2–L4, L1 maintains a higher missile–target relative velocity during the early guidance stage, which facilitates rapid interception. As shown in Figure 6(d)–(g), compared with L2–L4, the LOS elevation angle, LOS azimuth angle, and LOS angular rates under L1 converge more slowly; however, this does not affect the satisfaction of the desired impact angles at interception. As shown in Figure 6(h), acceleration saturation occurs for L2 and L3 at 10s, whereas the curves of L1 and L4 remain smooth and stable. As shown in Figure 6(i),(j), L2–L4 exhibit acceleration saturation in the initial guidance stage, and their acceleration profiles vary with relatively large amplitudes, imposing considerable stress on the onboard actuators. In contrast, L1 keeps the acceleration magnitude within a reasonable range, without acceleration saturation or

chattering, and thus better meets the engineering requirements. As summarized in Table 5, the miss distances of L1–L4 are all within 1 m. Although the missile–target relative velocity error, the LOS elevation angle error, and the LOS azimuth angle error of L1 are not as small as those of L2–L4, they remain at the order of E-02 or lower, which is sufficient to achieve the guidance objective. Moreover, the total flight time of L1 (23.402 s) is significantly shorter than those of L2–L4 (32.277 s, 32.984 s, and 30.398 s). If the initial missile–target distance is increased, the difference in flight time will become even more pronounced.

Therefore, compared with the guidance laws corresponding to L2–L4, the proposed guidance law can reach the target accurately with the desired impact velocity and impact angles in a shorter time, while reducing the load on the onboard actuators and enhancing the stability of the guidance process. By improving the double-power reaching law via the adaptive gain designed in this paper, the guidance performance of the missile delivering a deployable sonar device is significantly enhanced.

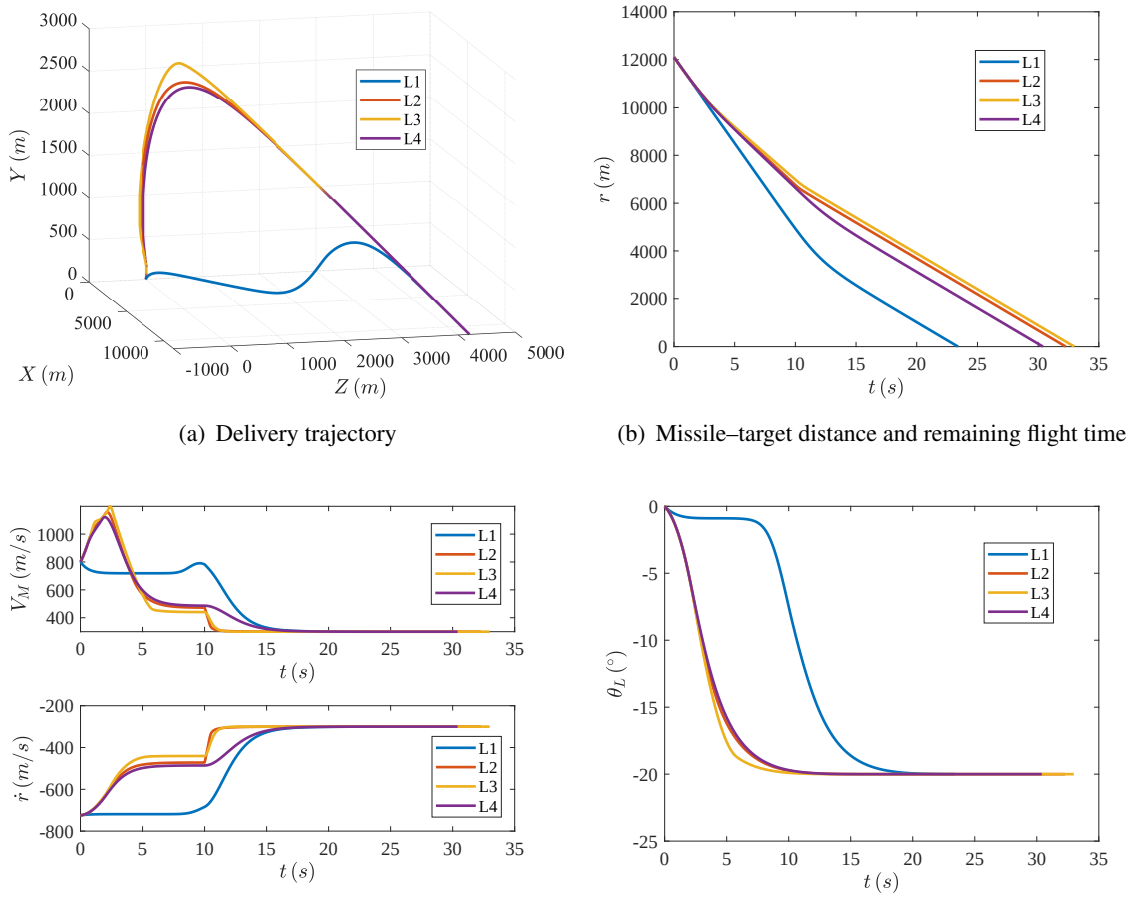

(a) Delivery trajectory

(b) Missile–target distance and remaining flight time

(c) Missile velocity and missile–target relative velocity

(d) LOS elevation angle

Figure 6. Guidance for the missile delivering a deployable sonar device based on different reaching laws.

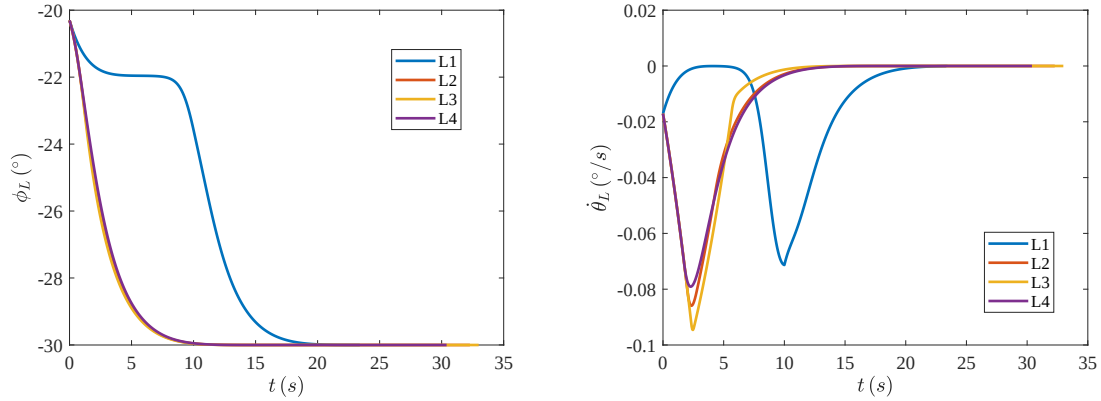

(e) LOS azimuth angle

(f) LOS elevation angular rate

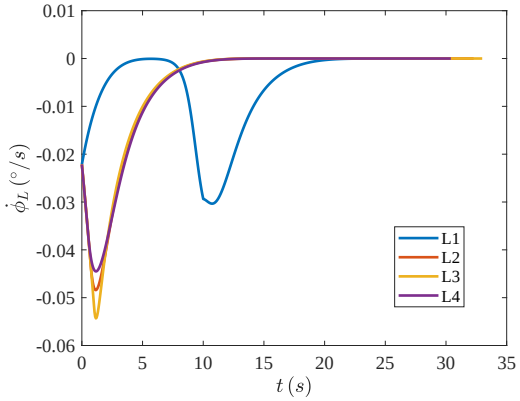

(g) LOS azimuth angular rate

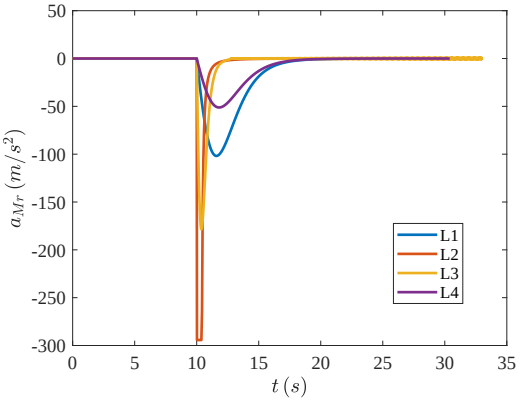

(h) LOS acceleration

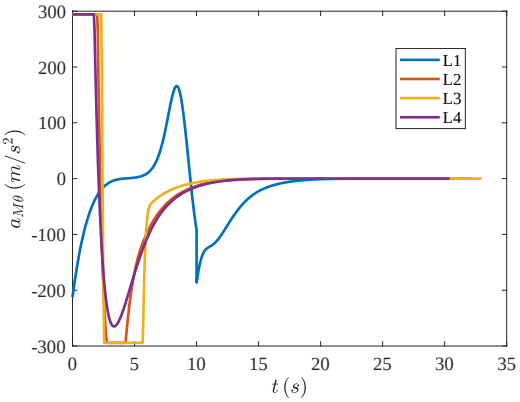

(i) LOS normal acceleration

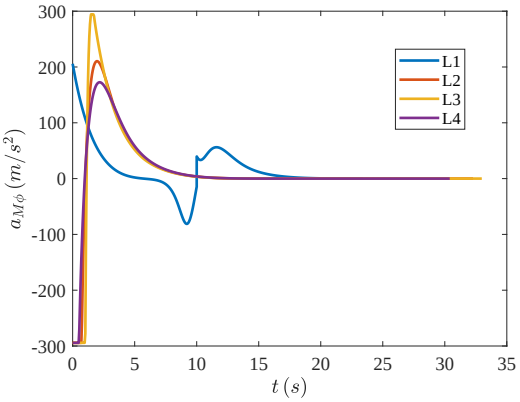

(j) LOS lateral acceleration

Figure 6. Guidance for the missile delivering a deployable sonar device based on different reaching laws.

Table 5. Simulation results of guidance based on different reaching laws.

Parameter	Value	Parameter	Value	Parameter	Value
$\theta_{Ld}(^\circ)$	Miss distance (m)	$\dot{r}$ error (m/s)	θ_L error ($^\circ$)	ϕ_L error ($^\circ$)	Flight time (s)
-25	0.75391	-5.6521E-02	1.4291E-03	1.0412E-04	23.402
-20	0.9079	-6.1959E-11	-3.9563E-11	-5.8895E-11	32.277
-15	0.75817	3.227E-04	-2.6687E-12	-4.0059E-11	32.984
-10	0.72085	5.6843E-14	3.5479E-11	1.96E-11	30.398

4.5. Monte Carlo simulation test

To evaluate the adaptability and robustness of the proposed adaptive two-phase guidance law for the missile delivering a deployable sonar device, this section conducts Monte Carlo simulation tests using the sliding surfaces, reaching laws, and control laws in Section 4.3, under the baseline engagement condition with $\theta_{Ld} = -20^\circ$ and $\phi_{Ld} = -30^\circ$. During the simulations, random disturbances are introduced into the engagement scenario, including initial target position deviations of ±1000 m in the longitudinal and lateral directions, variations of ±20 m/s in the initial missile speed, perturbations of ±5° in the initial missile pitch and yaw angles, and perturbations of ±5° in the desired terminal LOS angles. In addition, to account for sensor measurement errors, zero-mean Gaussian measurement noise is added to the seeker outputs, where the standard deviations of the range, missile–target relative velocity, LOS angles, and LOS angular rates are set to 2 m, 1 m/s, 0.005 rad, and 0.005 rad/s, respectively. The simulation is terminated when $r < 1$ m and $\dot{r} > 0$ m/s. Under these conditions, 500 Monte Carlo runs are performed, and the results are shown in Figure 7.

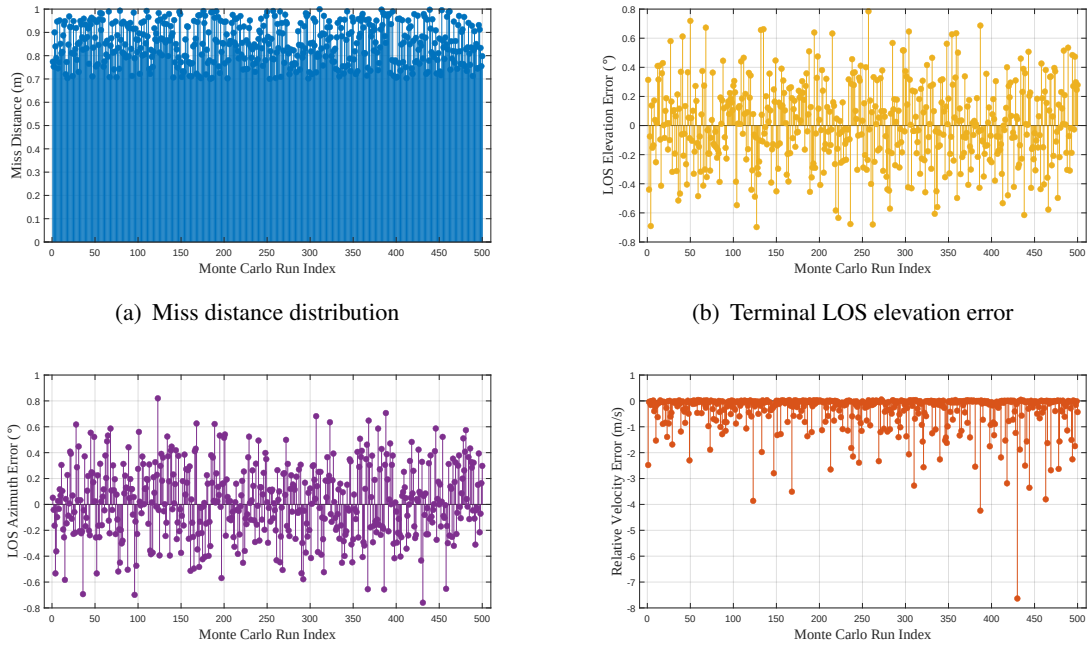

(a) Miss distance distribution

(b) Terminal LOS elevation error

(c) Terminal LOS azimuth error

(d) Terminal relative velocity error

Figure 7. Monte Carlo simulation test results.

In the test results, the mean miss distance is 0.8522 m, the mean terminal relative velocity error is −0.4059 m/s, the mean terminal LOS elevation angle error is 0.0087°, and the mean terminal LOS azimuth angle error is 0.0213°. As shown in Figure 7(b),(c), the distributions of the terminal LOS angle errors are relatively uniform with small fluctuations, and the maximum error is less than 1°, indicating that the designed impact angle constraint can be satisfied stably under random disturbances. As shown in Figure 7(d), although the terminal relative velocity error approaches −8 m/s in a few samples, the overall distribution remains mainly concentrated near zero, demonstrating that the impact velocity constraint also exhibits satisfactory enforcement performance. Overall, the Monte Carlo results indicate that, under the combined effects of initial-state perturbations, terminal LOS angle perturbations, and measurement noise, the proposed guidance law can drive the missile delivering a deployable sonar device to accurately reach the target with the desired impact angles and impact velocity, thereby validating the robustness of the proposed method in the presence of combined multi-source disturbances.

5. Conclusions

This paper innovatively proposes the concept of a missile delivering a deployable sonar device to cope with increasingly complex sea conditions. The missile can rapidly deliver the deployable sonar device to the target sea area, thereby enabling timely monitoring of the target's activities. For the missile delivering a deployable sonar device, a three-dimensional adaptive guidance law with fixed-time convergence is developed. To reduce the impact kinetic energy at water entry and to deploy the sensing device with a prescribed attitude, constraints on the water-entry velocity and water-entry angle are imposed. To avoid range unreachability induced by deceleration-based guidance laws and to prevent excessive flight time, a two-phase guidance strategy with smooth switching is designed along the LOS direction. To further enhance the stability of the guidance process, an adaptive term is incorporated into the double-power reaching law to alleviate early-stage acceleration saturation. To verify the superior performance of the proposed adaptive two-phase guidance law for the missile delivering a deployable sonar device, five groups of simulation tests are conducted.

By comparing the first three simulation cases, it is verified that two-phase guidance reduces the total flight time relative to full-phase guidance; it is also verified that the smoothly varying function designed in this paper can avoid abrupt jumps in the acceleration command during phase switching, thereby ensuring a bumpless transfer; moreover, it is confirmed that, after improving the double-power reaching law using the adaptive gain designed in this paper, the early-stage acceleration saturation can be alleviated and the flight time can be further reduced. The fourth simulation case further illustrates the advantages of the reaching law designed in this paper in a more direct manner. In addition, the Monte Carlo simulation tests further demonstrate that the proposed guidance law exhibits good adaptability and stability under random disturbances. Therefore, the proposed guidance law can accomplish the delivery mission of the deployable sonar device in a more efficient and stable way.

Under increasingly complex sea conditions, compared with anti-submarine helicopter and unmanned aerial vehicle platforms, the delivery approach investigated in this paper shows certain advantages in maneuverability and flexible deployment, and it has potential application value in adapting to different meteorological conditions, reducing reliance on real-time human intervention, and improving mission responsiveness, providing a feasible perspective for rapid delivery of a deployable

sonar device to a target sea area.

Future work: Although the proposed adaptive two-phase guidance law can reduce the overload at water entry, the missile's structure must be carefully designed to ensure safe and reliable deployment of the deployable sonar device. Future research can focus on the hardware and structural design of the missile delivering a deployable sonar device. In addition, the present work mainly focuses on the structural design and convergence properties of the guidance law, and the current validation is still based on an idealized relative-kinematics model. Important higher-fidelity engineering factors, such as autopilot dynamics, seeker dynamics, aerodynamic uncertainties, and realistic actuator bandwidth/rate/saturation effects, are not explicitly incorporated at this stage. Therefore, the conclusions of this paper should be interpreted as showing the feasibility of simultaneously enforcing impact velocity and impact angle constraints, as well as the potential to reduce early-stage control peaks, at the current kinematic modeling level, rather than as definitive conclusions for a complete engineering system.

Author contributions

Jian Huang: Conceptualization, validation, data curation, writing – original draft, and visualization; Zhanpeng Gao: Methodology and software.; Jun Liu: Formal analysis and writing – review; Wenjun Yi: Editing and supervision. All authors have read and approved the final version of the manuscript for publication.

Use of Generative AI tools declaration

The authors declare they have not used artificial intelligence (AI) tools in the creation of this article.

Acknowledgments

This work was supported by the National Natural Science Foundation of China (grant number: 62203191).

Conflict of interest

All authors declare no conflicts of interest in this paper.

References

1. W. Bi, J. Zhou, J. Shen, A. Zhang, Optimization method of passive omnidirectional buoy array in on-call anti-submarine search based on improved NSGA-II, *Ocean Eng.*, **293** (2024), 116655. https://doi.org/10.1016/j.oceaneng.2023.116655
2. Y. Yan, Y. Liu, Y. Bi, Q. Wang, H. Cao, Z. Yu, et al., Research on anti-submarine warfare method of unmanned aerial vehicle cluster based on area coverage and distributed optimization control, *Drones*, **8** (2024), 732. https://doi.org/10.3390/drones8120732

3. W. Yue, W. Tang, L. Wang, Multi-UAV cooperative anti-submarine search based on a rule-driven MAC scheme, *Appl. Sci.*, **12** (2022), 5707. https://doi.org/10.3390/app12115707
4. L. Jia, G. Zhang, Y. Liu, Z. Bai, Y. Geng, Y. Wu, et al., Sonar buoy active detection and localization for underwater targets using high-level sound sources and mems hydrophone, *Measurement*, **241** (2025), 115740. https://doi.org/10.1016/j.measurement.2024.115740
5. Z. Bai, G. Zhang, Y. Chai, G. Liu, Y. Liu, Y. Huang, et al., The study of baseline drift in mems sonar buoys, *Measurement*, **256** (2025), 118137. https://doi.org/10.1016/j.measurement.2025.118137
6. O. Thuillier, N. Le Josse, A. L. Olteanu, M. Sevaux, H. Tanguy, Efficient configuration of heterogeneous multistatic sonar networks: A mixed-integer linear programming approach, *Comput. Oper. Res.*, **167** (2024), 106637. https://doi.org/10.1016/j.cor.2024.106637
7. C. M. Taylor, S. Maskell, J. F. Ralph, Using hybrid multiobjective machine learning to optimise sonobuoy placement patterns, *IET Radar, Sonar Nav.*, **17** (2023), 374–387. https://doi.org/10.1049/rsn2.12347
8. Y. Shi, G. Wang, G. Pan, Experimental study on cavity dynamics of projectile water entry with different physical parameters, *Phys. Fluids*, **31** (2019), 067103. https://doi.org/10.1063/1.5096588
9. L. Sun, D. Wang, Y. Chen, G. Wu, Numerical and experimental investigation on the oblique water entry of cylinder, *Sci. Prog.*, **103** (2020). http://dx.doi.org/10.1177/0036850420940889
10. X. Liu, J. Xin, X. Chang, F. Shi, Z. Chen, Y. Wu, Dynamic and ricochet behaviors of a projectile for low-speed oblique water entry, *Results Eng.*, **28** (2025), 107274. https://doi.org/10.1016/j.rineng.2025.107274
11. X. Liu, X. Cai, Z. Huang, Y. Hou, J. Qin, Z. Chen, Comparative study on the oblique water-entry of high-speed projectile based on rigid-body and elastic-plastic body model, *Def. Technol.*, **46** (2025), 133–155. https://doi.org/10.1016/j.dt.2024.11.007
12. K. Ding, P. Shi, Y. Zhao, X. Wu, Y. Huang, T. Huang, Intermittent dynamic output feedback control for state-based stochastic switched systems and its application to electronic circuits, *IEEE T. Circuits-I*, **72** (2025), 7332–7345. https://doi.org/10.1109/TCSI.2025.3566724
13. G. Wu, X. Wu, J. Cao, W. Zhang, Event-triggered aperiodic intermittent control for linear time-varying systems, *ISA T.*, **144** (2024), 96–104. https://doi.org/10.1016/j.isatra.2023.11.005
14. D. He, H. Wang, Y. Tian, R. E. Precup, Model-free global sliding mode control using adaptive fuzzy system under constrained input amplitude and rate for mechatronic systems subject to mismatched disturbances, *Inform. Sci.*, **697** (2025), 121769. https://doi.org/10.1016/j.ins.2024.121769
15. Y. Zheng, Y. Xia, K. Li, H. Zhou, R. E. Precup, Boundary-aware sliding prescribed performance control for PMSMs under compound uncertainties, *Expert Syst. Appl.*, **304** (2026), 130786. https://doi.org/10.1016/j.eswa.2025.130786
16. Y. Weng, X. Gao, Data-driven sliding mode control of unknown MIMO nonlinear discrete-time systems with moving PID sliding surface, *J. Franklin I.*, **354** (2017), 6463–6502. https://doi.org/10.1016/j.jfranklin.2017.07.022
17. L. Zhou, Z. Q. Li, H. Yang, Y. T. Fu, H. Wang, Data-driven integral sliding mode control based on disturbance decoupling technology for electric multiple unit, *J. Franklin I.*, **360** (2023), 9399–9426. https://doi.org/10.1016/j.jfranklin.2023.07.005

18. Z. Ma, Q. Wang, H. Chen, A joint guidance and control framework for autonomous obstacle avoidance in quadrotor formations under model uncertainty, *Aerosp. Sci. Technol.*, **138** (2023), 2023. https://doi.org/10.1016/j.ast.2023.108335

19. Z. Ma, J. Wang, Y. Liang, D. Zhou, H. Chen, Real-time fault-tolerant guidance for launch vehicle ascending flight under thrust drop failure, *Acta Astronaut.*, **224** (2024), 338–352. https://doi.org/10.1016/j.actaastro.2024.08.012

20. J. Xie, K. Ma, Suboptimal guidance law against maneuvering target with time and angle constraints, *Aerosp. Sci. Technol.*, **148** (2024), 109111. https://doi.org/10.1016/j.ast.2024.109111

21. Z. Chen, A. Y. Krasnov, Disturbance observer based fixed time sliding mode control for a class of uncertain second-order nonlinear systems, *AIMS Math.*, **10** (2025), 6745–6763. https://dx.doi.org/2010.3934/math.2025309

22. Z. Liu, Z. Gao, High-reliability cooperative guidance law design considering link failure and input saturation, *AIMS Math.*, **11** (2026), 2430–2457. https://doi.org/10.3934/math.2026099

23. X. Wang, Y. Zhang, H. Wu, Sliding mode control based impact angle control guidance considering the seeker's field-of-view constraint, *ISA T.*, **61** (2016), 49–59. https://doi.org/10.1016/j.isatra.2015.12.018

24. Z. Gao, W. Yi, Integrated guidance and control design based on optimized sparrow search algorithm for sliding mode PID controller parameters, *Int. J. Aeronaut. Space*, **27** (2026), 791–810. https://doi.org/10.1007/s42405-025-00959-x

25. H. Zheng, Q. Wang, Z. Gong, H. Tang, H. Jiang, B. Zhou, Impact time and angle control guidance with terminal speed constraint based on periodic delayed feedback, *IFAC-PapersOnLine*, **59** (2025), 982–986. https://doi.org/10.1016/j.ifacol.2025.11.281

26. X. Wang, X. Huang, S. Ding, Terminal angle constraint finite-time guidance law with input saturation and autopilot dynamics, *J. Franklin I.*, **359** (2022), 8687–8712. https://doi.org/10.1016/j.jfranklin.2022.08.046

27. F. Dong, X. Zhang, P. Tan, Non-singular terminal sliding mode cooperative guidance law under impact angle constraint, *J. Franklin I.*, **361** (2024), 107079. https://doi.org/10.1016/j.jfranklin.2024.107079

28. Z. Hu, W. Yi, L. Xiao, Deep reinforcement learning-based impact angle-constrained adaptive guidance law, *Mathematics*, **13** (2025). https://doi.org/10.3390/math13060987

29. X. Yang, Y. Zhang, S. Song, Three-dimensional nonsingular impact angle guidance strategy with physical constraints, *ISA T.*, **131** (2022), 476–488. https://doi.org/10.1016/j.isatra.2022.05.023

30. Z. Hou, X. Zhuang, H. Chen, Nonlinear three dimensional all-aspect guidance with terminal impact angle constraints, *Aerosp. Sci. Technol.*, **142** (2023), 108602. https://doi.org/10.1016/j.ast.2023.108602

31. Z. Gao, W. Yi, J. Huang, J. Liu, Three-dimensional guidance law with precise control of attack time and constraints on attack angle, *ISA T.*, **167** (2025), 1228–1240. https://doi.org/10.1016/j.isatra.2025.09.028

32. H. Li, R. Zhang, Q. Wang, X. Lü, J. Yu, X. Dong, Three-dimensional helical guidance with impact time constraints, *IEEE T. Aero. Elec. Syst.*, **62** (2026), 253–268. https://doi.org/10.1109/TAES.2025.3621404

33. A. Huang, X. Wang, Q. Zhao, J. Yu, X. Dong, Three-dimensional practical cooperative guidance law for salvo attack considering velocity variation, *Aerosp. Sci. Technol.*, **166** (2025), 110588. https://doi.org/10.1016/j.ast.2025.110588

34. A. Huang, H. Li, Q. Wang, J. Yu, X. Dong, Integrated spatiotemporal guidance and decision-making design via distributed optimization strategy, *Control Eng. Pract.*, **164** (2025), 106469. https://doi.org/10.1016/j.conengprac.2025.106469

35. Y. Li, M. Zhu, B. An, Y. Zhi, L. Liu, H. Fan, et al., Three-dimensional cooperative guidance laws with impact velocity and impact angles constraints, *Aerosp. Sci. Technol.*, **159** (2025), 109997. https://doi.org/10.1016/j.ast.2025.109997

36. Z. Gao, J. Liu, J. Huang, W. Wang, W. Yi, S. Yuan, Three-dimensional fault-tolerant cooperative guidance law with constraints on relative impact velocity and attack angle, *Aerosp. Sci. Technol.*, **168** (2026), 111003. https://doi.org/10.1016/j.ast.2025.111003

37. Y. Liu, D. Yu, Q. Jia, Dynamic event-triggered prescribed-time cooperative guidance law for salvo attack with impact angle constraints, *Aerosp. Sci. Technol.*, **168** (2026), 110873. https://doi.org/10.1016/j.ast.2025.110873

38. H. Shen, H. Jiang, Y. Cai, Y. Deng, Three-dimensional prescribed-time cooperative guidance with neural network-based disturbance observer and LOS constraint, *Control Eng. Pract.*, **165** (2025), 106599. https://doi.org/10.1016/j.conengprac.2025.106599

39. W. Dong, C. Wang, J. Wang, Z. Zuo, J. Shan, Fixed-time terminal angle-constrained cooperative guidance law against maneuvering target, *IEEE T. Aerosp. Electron. Syst.*, **58** (2022), 1352–1366. https://doi.org/10.1109/TAES.2021.3113292

40. Z. Chen, W. Chen, X. Liu, J. Cheng, Three-dimensional fixed-time robust cooperative guidance law for simultaneous attack with impact angle constraint, *Aerosp. Sci. Technol.*, **110** (2021), 106523. https://doi.org/10.1016/j.ast.2021.106523

41. L. Yang, J. Yang, Nonsingular fast terminal sliding-mode control for nonlinear dynamical systems, *Int. J. Robust Nonlin.*, **21** (2011), 1865–1879. https://doi.org/10.1002/rnc.1666

42. Z. Liu, X. Gong, J. Fei, Nonsingular fast terminal sliding mode control of DC-DC buck converter using fuzzy neural network and disturbance observer, *Nonlinear Dynam.*, **113** (2025), 13389–13414. https://doi.org/10.1007/s11071-024-10857-8

43. H. You, X. Chang, J. Zhao, S. Wang, Y. Zhang, Three-dimensional impact-angle-constrained cooperative guidance strategy against maneuvering target, *ISA T.*, **138** (2023), 262–280. https://doi.org/10.1016/j.isatra.2023.02.030

44. S. P. Bhat, D. S. Bernstein, Finite-time stability of continuous autonomous systems, *SIAM J. Control Optim.*, **38** (2000), 751–766. https://doi.org/10.1137/S0363012997321358

45. E. Moulay, W. Perruquetti, Finite time stability and stabilization of a class of continuous systems, *J. Math. Anal. Appl.*, **323** (2006), 1430–1443. https://doi.org/10.1016/j.jmaa.2005.11.046

46. F. Dong, X. Zhang, K. He, P. Tan, A new three-dimensional adaptive sliding mode guidance law for maneuvering target with actuator fault and terminal angle constraints, *Aerosp. Sci. Technol.*, **131** (2022), 107974. https://doi.org/10.1016/j.ast.2022.107974

47. K. Zhao, J. Song, Y. Liu, Spatial-temporal cooperative guidance with no-fly zones avoidance, *Control Eng. Pract.*, **154** (2025), 106162. https://doi.org/10.1016/j.conengprac.2024.106162

AIMS Press